Aerosol Science and Technology, 41:295–314, 2007

ISSN: 0278-6826 print / 1521-7388 online
DOI: 10.1080/02786820701197078

An Inter-Comparison of Instruments Measuring Black Carbon Content of Soot Particles

Jay G. Slowik,[1] Eben S. Cross,[1] Jeong-Ho Han,[1] Paul Davidovits,[1] Timothy B. Onasch,[2] John T. Jayne,[2] Leah R. Williams,[2] Manjula R. Canagaratna,[2] Douglas R. Worsnop,[2] Rajan K. Chakrabarty,[3] Hans Moosmüller,[3] William P. Arnott,[3] Joshua P. Schwarz,[4] Ru-Shan Gao,[4] David W. Fahey,[4] Gregory L. Kok,[5] and Andreas Petzold[6]

[1]*Boston College, Chestnut Hill, Massachusetts, USA*
[2]*Aerodyne Research, Inc., Billerica, Massachusetts, USA*
[3]*Desert Research Institute of the Nevada System of Higher Education, Reno, Nevada, USA*
[4]*NOAA Earth System Research Laboratory, Chemical Sciences Division, Boulder, Colorado, USA*
[5]*Droplet Measurement Technologies, Boulder, Colorado, USA*
[6]*Institut für Physik der Atmosphäre, Deutsches Zentrum für Luft- und Raumfahrt Oberpfaffenhofen, Wessling, Germany*

Inter-comparison studies of well-characterized fractal soot particles were conducted using the following four instruments: Aerosol Mass Spectrometer-Scanning Mobility Particle Sizer (AMS-SMPS), Single Particle Soot Photometer (SP2), Multi-Angle Absorption Photometer (MAAP), and Photoacoustic Spectrometer (PAS). These instruments provided measurements of the refractory mass (AMS-SMPS), incandescent mass (SP2) and optically absorbing mass (MAAP and PAS). The particles studied were in the mobility diameter range from 150 nm to 460 nm and were generated by controlled flames with fuel equivalence ratios ranging between 2.3 and 3.5. The effect of organic coatings (oleic acid and anthracene) on the instrument measurements was determined. For uncoated soot particles, the mass measurements by the AMS-SMPS, SP2, and PAS instruments were in agreement to within 15%, while the MAAP measurement of optically-absorbing mass was higher by ∼50%. Thin organic coatings (∼10 nm) did not affect the instrument readings. A thicker (∼50 nm) oleic acid coating likewise did not affect the instrument readings. The thicker (∼60 nm) anthracene coating did not affect the readings provided by the AMS-SMPS or SP2 instruments but increased the reading of the MAAP instrument by ∼20% and the reading of the PAS by ∼65%. The response of each instrument to the different particle types is discussed in terms of particle morphology and coating material.

Received 3 March 2006; accepted 4 January 2007.

Funding for this work was provided by the National Air and Space Administration (NASA) through the Upper Atmosphere Research Program contract NAG2-1462 and the Atmospheric Chemistry Program contract NNH04CC09C, by the Atmospheric Chemistry Program of the National Science Foundation (NSF) grant Nos. ATM-0212464 and ATM-0525355, by the Office of Biological and Environmental Research of the Department of Energy (Atmospheric Science Program) grant Nos. DE-FG02-98ER62581 and DE-FG02-05ER63995. JGS and ESC were funded by the NASA Earth System Science Fellowship program. JPS, RSG, and DWF were supported by the National Oceanic and Atmospheric Administration Climate Program. The SP2 was developed under an SBIR grant from the Office of Naval Research, No. N00014-01-C-0335, to Droplet Measurement Technologies. The contributions of the Desert Research Institute were supported in part by the DOE Atmospheric Science Program under grant DE-FG02-05ER64008, with additional support for instrument development from NSF under grants ATM-0340423 and ATM-9871192. The contribution of AP to the study was supported by the European project AERONET under contract No. ACA3-CT-2003-502882.

Address correspondence to P. Davidovits, Chemistry Department, Boston College, Merkert Chemistry Center 223, 140 Commonwealth Avenue, Chestnut Hill, MA 02467, USA. E-mail: paul.davidovits@bc.edu

INTRODUCTION

Soot particles contain as a major component a refractory, light-absorbing material often called black carbon[1] (BC) (Kleeman et al. 2000). This material largely determines the optical properties of soot particles and influences their chemical and morphological transformations. Because BC is an effective light absorber, internally and externally mixed aerosol containing BC contributes to climate change by direct radiative forcing (IPCC 2001). There are, however, questions about the magnitude of

[1]As is discussed in the recent review by Bond and Bergstrom (2006), the nomenclature for the light-absorbing, refractory component of carbonaceous aerosols is not clearly established. The term "black carbon" is often used in connection with the light-absorbing properties of the aerosol, while "elemental carbon" is often used when thermal properties are considered. Other terms, such as "graphitic carbon," which addresses properties of carbon atoms in a graphitic lattice, are also in use.

the heating effect (Penner et al. 2003; Johnson 2005). Black carbon-containing aerosols may be involved in the melting of polar ice (Hansen and Nazarenko 2004). Measurements of BC content in soot are required to provide quantitative data for the evaluation of the effect of BC-containing aerosols on global warming. Aged BC aerosols may acquire hydrophilic coatings and act as cloud or ice nuclei (Dusek et al. 2006).

Quantitative measurement of BC is challenging because BC often occurs in highly non-spherical soot particles of complex morphology (Park et al. 2003; Chakrabarty et al. 2006). The task is further complicated because of the lack of an unambiguous chemical definition of the material. Still, a number of techniques have been developed for measuring BC in particles based either on the thermal properties of BC or its optical properties. These two classes of measurement techniques do not necessarily yield the same results. Quantitative comparisons of the available techniques are an essential step in obtaining meaningful measurements of BC. Here we first provide a survey of the most commonly used techniques and then discuss the methods applied in the current studies.

Optical techniques are typically designed to measure light absorption by aerosols, which is then empirically related to BC content. The aethalometer is one such common instrument based on the optical properties of BC deposited on a filter (Hansen et al. 1984; Gundel et al. 1984; Arnott et al. 2005a). It determines absorption by impacting particles on a quartz fiber filter and measuring the change in light transmission as a function of time. The particle soot absorption photometer (PSAP) also performs a filter-based absorption measurement (Bond et al. 1999). Cavity ring-down techniques yield the aerosol extinction coefficient by measuring the time constant for light decay in a high finesse cavity containing the absorbing particles. In conjunction with a separate measurement of scattering coefficients with an instrument such as a nephelometer, the cavity ring-down techniques provide an in-situ measurement of the aerosol absorption coefficient (see for example Smith and Atkinson 2001; Sheridan et al. 2005; Moosmüller et al. 2005). Two other optically based instruments, the Photoacoustic Spectrometer (PAS) and the Multi-Angle Absorption Photometer (MAAP), are subjects of the present study and will be described in the following section. One drawback for all of these techniques is the need for an empirical conversion factor from optical response to BC mass. The conversion factor may depend on the composition and morphology of the particles used in the calibration of the instrument and on the specific technique used to quantify the BC mass.

Thermal-optical analysis techniques typically induce oxidation and/or evaporation of organic carbon (OC), and define black carbon as the remaining refractory component (see for example Fung 1990; Turpin et al. 1990; Viidanoja et al. 2002). An example of a class of such instruments is the thermal/optical reflectance carbon analyzer (TOR) developed by Huntzicker et al. (1982) in which OC and BC are distinguished by their volatility. The optical reflectance is used to account for the OC that is pyrolyzed (Chow et al. 1993; Moosmüller et al. 2001). Other techniques account for the OC component by measuring the amount of CO_2 generated as a function of temperature (e.g., Turpin et al. 1990). However, the existence of multiple protocols for the heating/oxidation process leads to significant uncertainty in the distinction between OC and BC provided by different instruments (Countess 1990; Schmid et al. 2001). Further, BC-like products of OC pyrolysis can lead to an overestimate of the BC mass. The analysis using these instruments is performed either as a batch process or with limited time resolution ($\sim$30 minutes).

Two techniques tested in the present study that do not fall clearly into either of the above categories are the Single Particle Soot Photometer (SP2) and a mass balance technique derived from tandem measurements with the Aerodyne Aerosol Mass Spectrometer and a Scanning Mobility Particle Sizer (AMS-SMPS). Both of these instruments are described in the following section. In the SP2, laser-induced incandescence is empirically related to BC mass. In the AMS-SMPS, the BC content is assumed to be the refractory component of the particles and is obtained by mass balance of the measured non-refractory organics and the total particle mass, which is derived from effective diameter measurements.

Several inter-comparisons of BC-measuring instruments have been previously conducted. A comparison at Colorado State University in 1980 of the then state-of-the-art techniques in optical and chemical measurement of BC showed measurement differences by about a factor of two to three among the optical instruments (Gerber 1982a, b). During the SCAR-B (Smoke, Clouds, and Radiation—Brazil) experiment in Brazil, biomass burning aerosols were analyzed by six methods (optical extinction cell, integrating plate, optical reflectance, particle soot absorption photometer (PSAP), thermal evolution, and remote sensing) and uncertainties in BC mass on the order of 20–40% were reported (Reid et al. 1998). The PSAP and integrating plate methods overestimated the BC content due to a significant response to non-absorbing particles (Bond et al. 1999; Horvath et al. 1997). At the AIDA (Aerosols, Interactions, and Dynamics in the Atmosphere) aerosol chamber (Karlsruhe, Germany) diesel particles and artificial spark-generated soot, in external mixtures with $(NH_4)_2SO_4$, were analyzed with several techniques, including photoacoustic spectrometry and aethalometry (Saathoff et al. 2003a). Significant differences in both particle morphology and optical properties were observed between the diesel and spark-generated soot. In a comparison of optical and thermal analysis techniques conducted on particles in urban and remote regions of Canada, Sharma et al. (2002) found that the conversion of optical data to BC mass needed to be adjusted for both the aethalometer and PSAP depending on the particle sources.

In the recent Reno Aerosol Optical Study (RAOS) (Sheridan et al. 2005; Arnott et al. 2005; Petzold et al. 2005), laboratory inter-comparison of aerosol light absorption measurements was made using a PAS, MAAP, PSAP, folded-path Optical Extinction Cell, three cavity ring-down extinction instruments, nephelometers, and optical particle counters. The laboratory aerosols studied were external mixtures in varying combinations

of $(NH_4)_2SO_4$ with either graphite particles or kerosene soot. Reference light absorption values were set as the average of photoacoustic measurements at 532 nm and a measurement derived from the difference of extinction and scattering measurements. The MAAP readings were in agreement with the reference absorption to within about 12% (Petzold et al. 2005). However, the accuracy of the PSAP readings showed a dependence on the aerosol single scattering albedo that could be traced to corrections needed in the filter loading algorithm. (Virkkula et al. 2005).

Here we report results from an inter-comparison study conducted at the Boston College laboratories during May 2005 utilizing the following four techniques: the Aerosol Mass Spectrometer-Scanning Mobility Particle Sizer (AMS-SMPS) (Slowik et al. 2004; DeCarlo et al. 2004), the Single Particle Soot Photometer (SP2) (Schwarz et al. 2006), the Multi-Angle Absorption Photometer (MAAP) (Petzold et al. 2002), and the Photoacoustic Spectrometer (PAS) (Arnott et al. 1999). An optical detection module in the AMS and a Scanning Electron Microscopy (SEM) sampling system were also employed. The MAAP and PAS represent filter and non-filter based absorption measurements, respectively. The SP2 and AMS-SMPS are measurements that do not fall clearly into any of the categories given above, although the AMS-SMPS is related to the thermal methods described in that it identifies BC as the refractory component of a particle.

An aim of the present study is to compare simultaneous measurements of refractory mass, measurements of incandescence, and measurements of optical absorption performed on the same ensemble of aerosols. All of these measurements can be reported in terms of mass, in which case we refer to the measured quantities as "refractory mass," "incandescent mass," or "optically absorbing mass." We expect that while perhaps not identical, the material responsible for all these properties is principally composed of carbon, with few attached hydrogens. When discussing the material responsible for these properties in a general way, we will refer to it as "black carbon" (BC). Commercially-produced carbon spheres are also utilized in this study. The material composing these particles is referred to as "glassy carbon" (GC).

The key and novel features of these inter-comparison experiments were the following: (1) Soot particles were well-characterized with respect to the source fuel-to-oxygen ratio, particle size, shape, fractal dimension, and composition. (2) The effect of controlled coatings composed of liquid oleic acid and solid anthracene on BC detection and particle light absorption was measured. (3) The measurement techniques investigated the black carbon content and optical properties of particles in real or near real-time in contrast to thermal/extraction filter techniques that require a significant delay and/or filter handling between collection and analysis. (4) The experiments specifically inter-compared measurements of light absorption, incandescent mass, and refractory mass. The studies test the common assumption that these quantities are approximately the same, and address some of the outstanding issues and assumptions incorporated in the operation of the selected instruments.

DESCRIPTION OF INSTRUMENTS

Aerosol Mass Spectrometer-Scanning Mobility Particle Sizer (AMS-SMPS)

The AMS-SMPS yields a measure of the refractory particle mass, which in this experiment is expected to be approximately equal to the BC mass. Detailed instrument descriptions are available in the literature for both the AMS (Jayne et al. 2000; Allan et al. 2003; Jimenez et al. 2003) and the SMPS (see for example Flagan 1999). Here we address only differences from standard instrument operation and the application of the instrument readings to the particles studied.

In the AMS, particles are sampled from a gas flow at ambient pressure into an aerodynamic lens (2 torr). The lens has the dual purpose of focusing the particles into a narrow beam and, by expansion into a vacuum system ($\sim 10^{-4}$ torr), accelerating them to a velocity inversely related to their vacuum aerodynamic diameter (d_{va}). The particles strike a heated surface where the non-refractory components are vaporized. The resulting gas is ionized by electron impact (45 eV) and detected by a quadrupole mass spectrometer at $\sim 10^{-7}$ torr. In one mode of operation, the particle d_{va} is obtained from the particle time-of-flight between a spinning chopper wheel near the outlet of the lens and the vaporizer surface. In a second mode of operation, the particle beam is alternately blocked and unblocked, yielding a quantitative mass spectrum of all non-refractory components. A mass spectral response is obtained in both modes of operation from the non-refractory flame-generated PAHs and aliphatics that are contained in all soot particles studied here.

The AMS used in this study is also equipped with an optical detection module, which functions as an additional detector when the AMS is used to size particles. This system provides the particle d_{va} for both refractory and non-refractory particles (Cross et al. 2007). This is a useful feature because the AMS alone does not respond to the glassy carbon spheres used in this study as calibrating particles for the SP2 instrument.

The SMPS part of the instrument is a combination of a differential mobility analyzer (DMA) (Model 3080, TSI Inc., St. Paul, MN, USA) and a condensation particle counter (CPC) (Model 3010, TSI inc., St. Paul, MN, USA). In the current experiments, the DMA scans through the particle size distribution with a period of two minutes, while the CPC counts the number of particles in each size bin. The scanning DMA is operated at a sheath/aerosol flow ratio of 10:1 (sheath flow = 3 L/min; aerosol flow = 0.3 L/min), yielding a DMA size transmission width of approximately $\pm 10\%$. The SMPS measures the mobility diameter (d_m) and total particle concentration in the flow. In cases where more than one particle mode is present, due to multiple charging of aerosol particles, the size distributions are corrected by an algorithm provided by the instrument manufacturer. An additional check on the particle concentration is obtained by comparison of the SMPS measurement with a stand-alone CPC.

The AMS alone cannot measure the refractory content of aerosol particles. To measure refractory content, the two normally stand-alone instruments, the AMS and the SMPS,

are combined to provide complementary information about the aerosol particles. The SMPS instrument provides the particle mobility diameter, d_m. The AMS yields the vacuum aerodynamic diameter, d_{va}. From the quantitative mass spectrum provided by the AMS and the total particle concentration provided by the SMPS, we obtain the per particle mass of each non-refractory component. The coupled AMS-SMPS measurements of d_m, d_{va}, and the non-refractory composition of the particles are used in Equations (1–3) to determine particle volume, shape, density, and composition (DeCarlo et al. 2004; Slowik et al. 2004).

$$d_m = \frac{d_{ve}\chi C_c(d_m)}{C_c(d_{ve})} \quad [1]$$

$$d_{va} = \frac{d_{ve}}{\chi\rho_0}\left(\frac{m_{REF}+m_{PAH}+m_{AL}+m_{COAT}}{\frac{m_{REF}}{\rho_{REF}}+\frac{m_{PAH}}{\rho_{PAH}}+\frac{m_{AL}}{\rho_{AL}}+\frac{m_{COAT}}{\rho_{COAT}}}\right) \quad [2]$$

$$m_{REF}+m_{PAH}+m_{AL}+m_{COAT} = \frac{\pi}{6}d_{ve}^3\left(\frac{m_{REF}+m_{PAH}+m_{AL}+m_{COAT}}{\frac{m_{REF}}{\rho_{REF}}+\frac{m_{PAH}}{\rho_{PAH}}+\frac{m_{AL}}{\rho_{AL}}+\frac{m_{COAT}}{\rho_{COAT}}}\right) \quad [3]$$

In these equations, d_{ve} is the volume equivalent diameter (defined as: particle volume $= \pi d_{ve}^3/6$), χ is the dynamic shape factor (defined as the ratio of the drag on a particle to the drag on a sphere with diameter d_{ve}), $C_c(d)$ is the Cunningham slip correction factor, ρ_0 is unit density (1.00 g cm^{-3}), ρ_{REF}, ρ_{PAH}, ρ_{AL}, and ρ_{COAT} are the material densities of the refractory component, flame-generated PAH, flame-generated aliphatics (AL), and coating material (if any), respectively (values for these densities are given in Table 1), and the "$m_{subscript}$" terms are the mass per particle for the individual species. Note that in Equations (2) and (3), the expression in parenthesis is equal to particle density, ρ_p. (That is, ρ_p = sum of component masses/sum of component volumes.) Equations (1–3) contain only measured quantities (d_{va}, d_m, and the non-refractory mass components), estimated quantities (material densities), and three unknowns (d_{ve}, χ, and m_{REF}). These equations are solved to yield the unknown values. Errors are calculated for each of the measured quantities in Equations (1–3) and propagated through the solution process via a sensitivity analysis. We report the error as 1 standard deviation.

TABLE 1
List of constants used in AMS-SMPS calculation of refractory mass (AL = aliphatics)

Constant	Value
Material density of black carbon (ρ_{BC})	1.8 g cm^{-3}
Material density of GC spheres (ρ_{GC})	1.5 g cm^{-3}
Material density of flame-generated PAHs (ρ_{PAH})	1.3 g cm^{-3}
Material density of flame-generated aliphatics (ρ_{AL})	0.8 g cm^{-3}
Material density of oleic acid (ρ_{OA})	0.9 g cm^{-3}
Material density of anthracene (ρ_{AN})	1.3 g cm^{-3}

The fractal dimension (D_f) is obtained from the mass-mobility relationship, given in Equation (4) (Park et al. 2003).

$$m_p = C' d_m^{D_f} \quad [4]$$

Here m_p is the particle mass, and C' is a proportionality constant. The fractal dimension has a maximum value of 3 (for a sphere) and a minimum value of 1 (for a linear chain of primary particles) (see for example DeCarlo et al. 2004).

It is shown in Slowik et al. (2004) that m_p as calculated by this method depends mostly on the measurements of d_m and d_{va} and does not depend strongly on ρ_p. For example, a 50% uncertainty in ρ_p results in an uncertainty of only about 10% in m_p. Therefore, even if the density of the refractory component is not well known or the particle contains more than one refractory species, the refractory mass can still be determined. However, the AMS-SMPS does not directly provide the chemical identity of the refractory material(s). As a result, for particles containing an unknown refractory component or a mixture of multiple refractory components in unknown proportions, the refractory volume, density of refractory material, and the relative amounts of the different refractory species remain unknown.

The AMS-SMPS measurement of refractory mass is similar in principle to the method used by Park et al. (2003), who obtained effective density by measuring mobility diameter, aerodynamic diameter, and particle mass.

Single Particle Soot Photometer (SP2)

The operating principles of the SP2 instrument are described elsewhere (Stephens et al. 2003; Baumgardner et al. 2004; Schwarz et al. 2006). Two SP2 instruments were used in these experiments; one operated by NOAA, the other by Droplet Measurement Technologies (DMT). Sample aerosol particles pass through an air jet and intersect an intense, intra-cavity, continuous Nd:YAG laser beam (1064 nm). Lenses on four separate optical axes capture light emitted or scattered by particles in the laser beam and image it onto avalanche photo-detectors (APD). Scattered laser light is used to size non-absorbing particles. In addition to scattering light, black carbon and other refractory particles absorb laser light, reach incandescence, and vaporize within the beam. In the NOAA SP2, two avalanche photo-detectors measure incandescent light over "broadband" (~350–800 nm) and "narrowband" (~630–800 nm) wavelength intervals defined with optical filters. The ratio of responses in the two detectors is related to the color temperature of the incandescing aerosol and can be used to determine the particle vaporization temperature. Vaporization temperature provides information about possible particle composition. (Stephens et al. 2003; Schwarz et al. 2006). The DMT instrument employed two filtered detectors, both in the 400–800 nm range. The peak incandescence signal is proportional to incandescent mass (this study and Schwarz

et al. 2006). The detector signals from individual particles are recorded and stored for analysis. The SP2 was calibrated during this study using glassy carbon spheres, which have a known density and can be size-selected with a DMA.

Multi-Angle Absorption Photometer (MAAP)

A detailed description of the MAAP is provided in the literature (Petzold et al. 2002; Petzold and Schönlinner 2004). In this instrument, particles are deposited on a quartz fiber filter. A continuous 670 nm laser is passed perpendicular through the filter matrix and the transmission is measured. The decrease in the transmitted light is due to two factors: (1) absorption by the particles on the filter and (2) scattering by the particles and filter matrix. Additional detectors placed at selected angles permit full characterization of the scattered light and thus allow the determination of the absorbance of the particle layer on top of the filter (Petzold and Schönlinner 2004). The aerosol absorption coefficient (B_{abs}) at 670 nm is calculated from absorbance and instrument geometry (Petzold et al. 2002). (B_{abs} is defined in terms of the fractional decrease in the light intensity (I/I_0) due to absorption and the optical path length (z) as $B_{abs} = -\ln(I/I_0)/z$.) For proper operation under the flow conditions in the present experiments, the internal plumbing of the commercial unit had to be modified. Such a modification does not affect the instrument response.

Calibration of B_{abs} with the VDI 2465 part 1 thermal reference method (VDI 2465 part 1, 1996) yields an empirically determined mass-specific aerosol absorption coefficient (σ_{abs}) (Petzold and Schönlinner 2004). In the VDI 2465 part 1 reference method, particles are collected on a filter, the organic carbon is removed by solvent extraction and thermal desorption, and the remaining BC is quantified by combustion. A narrow range of values for σ_{abs} (6.4–6.6 m^2g^{-1}) was found to provide a good fit to urban particles collected at several sites. A value of $\sigma_{abs} = 6.6$ m^2g^{-1} is currently used in the instrument. The parameters σ_{abs} and B_{abs} are used to calculate the instantaneous BC mass loading on the filter from the measured absorbance.

The B_{abs} and BC mass on the filter is monitored at a rate of 1 Hz. The flow rate carrying the particles through the filter is also measured. Together, these two measurements provide the mass concentration of BC ($\mu g/m^3$). In this experiment, a condensation particle counter (CPC) is used to normalize the measured BC mass loading to the particle number concentration. In this way, direct comparison with the SP2 and AMS-SMPS is made possible.

Photoacoustic Spectrometer (PAS)

A detailed description of the PAS is found in the literature (Arnott et al. 1999; Arnott et al. 2005b). In this instrument, particles are irradiated by laser light (870 nm) modulated at 1500 Hz. The corresponding heat produced within the particles by the absorbed laser light is rapidly transferred to the surrounding gas, producing an increase in pressure detected as a standing acoustic wave by a microphone (Arnott et al. 1999). This acoustic pressure is used together with instrument parameters to calculate the aerosol absorption coefficient (B_{abs}) (Rosencwaig 1980; Arnott et al. 1999; Arnott et al. 2000). The parameter B_{abs} has been empirically related to the BC mass concentration by a mass-specific absorption coefficient (σ_{abs}) obtained by calibration with a thermal/optical reflectance carbon analyzer (Chow et al. 1993; Moosmüller et al. 2001). For the wavelength used in the current study (870 nm), a value of $\sigma_{abs} = 6.2$ m^2 g^{-1} is used.

Because the PAS provides a non-destructive measurement of particle absorption and BC content, it can be used in series with other instruments. In the present studies, the MAAP instrument followed the PAS. The insertion of the PAS does not result in detectable particle losses. As with the MAAP instrument, here also the condensation particle counter (CPC) is used to normalize the measured BC mass loading to the number of particles for comparison with the SP2 and AMS-SMPS.

PARTICLE GENERATION

Uncoated Soot

A schematic of the apparatus for the inter-comparison studies is shown in Figure 1. Particles were generated in a commercially available McKenna burner by the combustion of a mixture of C_2H_4 (ethylene) and O_2 premixed with a dilution flow of N_2 and surrounded by a sheath flow of N_2. To achieve the range of flame and particle properties desired, the ethylene flow was varied between 1.8 and 4.2 L/min, the O_2 flow between 2.2 and 4.5 L/min, and the dilution N_2 between 2.2 and 4.7 L/min. The N_2 sheath flow was held constant at 25.4 L/min. The particles were sampled through an inlet consisting of two concentric stainless steel tubes (see inset to Figure 1). Particles were carried up the inner tube while a separate carrier gas (N_2) flow (14.5 L/min) was passed down the outer tube and then back up the inner tube, as shown. The gas flow around the lip of the inner tube prevents soot buildup in this region and dilutes the particle concentration. The gas flow was then passed through an impactor to remove particles larger than about 5 μm. At this point, most of the gas flow was diverted by a pump with only a small fraction (5–10%, depending on flame conditions) sampled into the system.

In order to generate a monodisperse particle size distribution, two DMAs were used. In a DMA, the particles are sized by their electric mobility, which is related to particle mobility diameter (d_m) divided by charge (q). If particles with mobility diameter d_m and $q = 1$ are selected, then particles with mobility diameter $2 \times d_m$ and $q = 2$, $3 \times d_m$ and $q = 3$, and so on are also transmitted. Therefore, at any instrument setting, multiple particle size modes may be transmitted by the DMA. Because the polydisperse size distribution is determined by the flame conditions, the number of modes and fraction of particles in each mode depend on both the selected d_m and flame conditions. The number of transmitted modes is limited by the range of the polydisperse size distribution. In the present experiment, it was common to

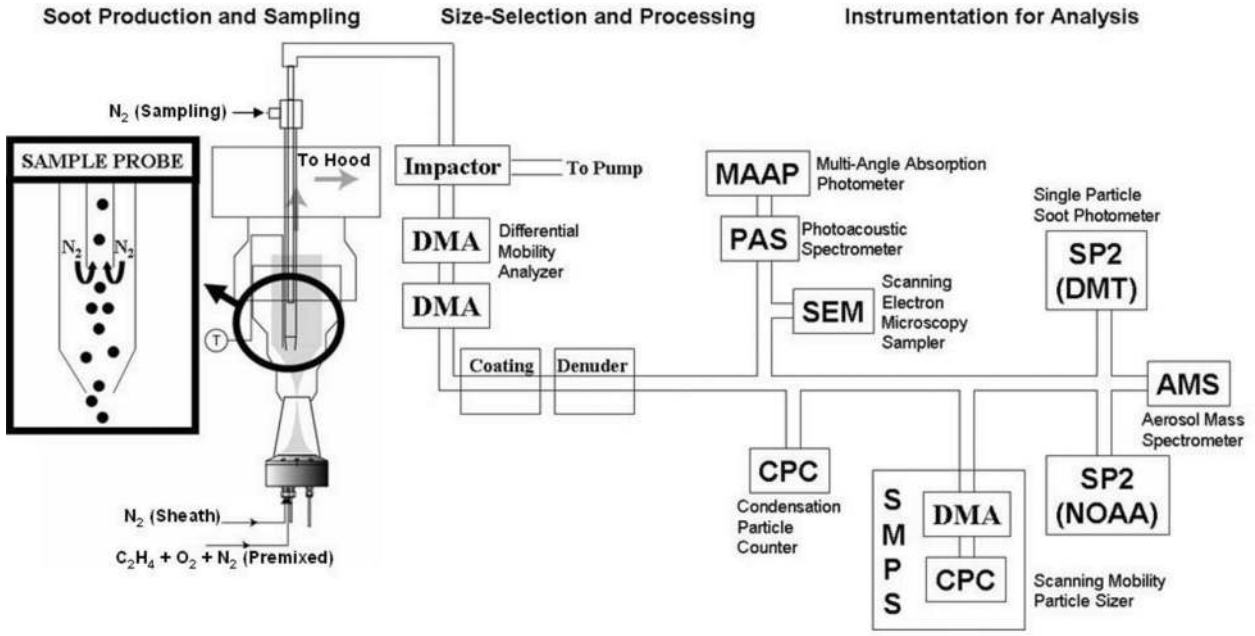

FIG. 1. Apparatus for soot production, processing, and analysis. Particles, continuously produced at the burner, flow through the system. Where the particle flow is split, sampling is performed isokinetically to avoid distortion of particle size distribution.

find 3 particle modes transmitted by the first DMA. The second DMA was set to select only the $q = 2$ particles transmitted by the first DMA (excluding the $q = 1$ and $q = 3$ modes).

The second DMA was not used at the beginning of the study. Although the addition of the second DMA improved the size distributions, modes other than the selected size modes still contributed significantly to the total mass. The second DMA improved the monodisperse character of the particle size distributions from ~60% (± 25%) by volume to ~80% (± 20%). There was no systematic difference in the results using the two setups. Therefore, no distinction between the data obtained with the two setups was made in the data analysis. A sample SMPS size distribution is shown in Figure 2 for particles produced at $\phi = 3.5$ and $d_m \sim 190$ nm. The second peak in the figure are the particles transmitted by the size-selecting DMAs at $q = 2$. The diameter of these particles is approximately 380 nm.

Due to the flow requirements of the system and the need to sample particles of a large size, the sheath/aerosol flow rate in the DMA (one or both) was ~4:1 (sheath flow ~8 L/min; aerosol flow ~2 L/min). Under these flow conditions, the resolution of the DMA instruments is approximately ± 30%. The series combination of the two DMA instruments yields a resolution of approximately ± 20%. After size-selection, the flow was isokinetically split and passed into the sampling instrumentation where BC content and optical properties were measured.

Coated Soot

Soot particles were produced by the method described in the previous section. After size-selection, the particles were passed over a heated reservoir of the specific organic species. The coatings studied in these experiments were oleic acid (a liquid organic acid) and anthracene (a solid polycyclic aromatic hydrocarbon). The organic vapor was entrained in the particle stream, and the mixture was cooled to room temperature, causing the vapor to condense on the particles. The thickness of coating was controlled by the reservoir temperature. The particles were analyzed by the instrumentation shown in Figure 1.

For the higher oleic acid temperatures, some nucleation of pure oleic acid particles was observed. Under these circumstances, the SMPS number distribution was used to correct the

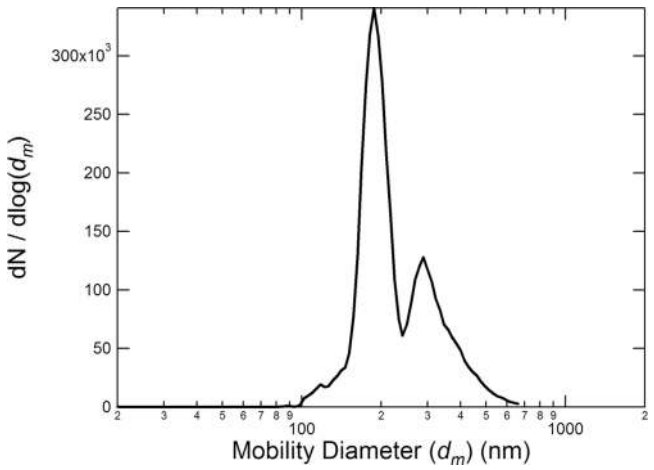

FIG. 2. Sample SMPS size distribution for particles produced at $\phi = 3.5$ and selected at $d_m \sim 190$ nm.

CPC measurement to provide a count for only the coated soot particles. This corrected CPC measurement was used to derive the mass per particle from the MAAP and PAS as described in the Experimental Results section.

Glassy Carbon Spheres

In addition to the flame-generated soot described above, studies were also conducted with commercially-produced glassy carbon (GC) spheres (Glassy Carbon Spheres, Type II, Alfa Aesar, Ward Hill, MA, USA). The GC spheres were suspended in water and atomized by a TSI Model 3076 Constant Output Atomizer (TSI, St. Paul, MN, USA). The particles were dried in a diffusion dryer containing anhydrous calcium sulfate (Drierite, Aldrich, Milwaukee, WI, USA). Dried particles with mobility diameters of 160, 205, 290, 315, 420, and 465 nm were selected, though other sizes were present due to the multiply charged particles passed by the DMA as described earlier. After size-selection, the particles were analyzed by the instrumentation shown in Figure 1. The particles were spherical and had a manufacturer-reported density of 1.42 g/cm^3. This density was confirmed using tandem measurements of the AMS and SMPS. Because the particles are spherical and have no internal voids, d_{va}/d_m equals both the particle density and material density. The d_{va}/d_m measurement yielded a density of 1.42 ± 0.09 g/cm^3. The refractive index of the GC spheres is unknown. A value of $n = 2 + i1$ was assumed for Mie scattering calculations by Gao et al. (2007).

SOOT PARTICLE CHARACTERIZATION

The particles were characterized in terms of their size, shape, fractal dimension, and composition by the AMS-SMPS. Details of the characterization procedure are found in Slowik et al. (2004) and were summarized in the previous section.

Uncoated Soot

The properties of the flame-generated soot particles depend on the fuel equivalence ratio (ϕ) of the flame, defined as $\phi =$ (molecular fuel/O_2 ratio in the flame)/(molecular fuel/O_2 ratio for complete combustion to CO_2 and H_2O). Soot particles were produced from flames at five fuel equivalence ratios ($\phi = 2.3$, 2.8, 3.5, 5.0, and 6.0). Flames with $\phi \leq 4$ produce soot consisting of fractal aggregates of BC spherules, while flames with $\phi > 4$ produce near-spherical soot with similar amounts of BC and non-refractory organics, with a near-step transition at $\phi =$ 4.0 (Slowik et al. 2004). Unfortunately, due to the flow and particle concentration requirements of the various instruments, the soot sampling apparatus was run under conditions that necessitated a higher-than-optimal flowrate through the sampling probe shown in the inset to Figure 1. At the high flowrates used in this experiment, the sampled region of the flame was geometrically large enough to encompass a range of flame conditions due to dilution from the N_2 sheath flow. As a result, at $\phi \geq 4$ a significant number of fractal particles were mixed with the non-fractal ones. The mixed fractal and near-spherical particles, along with the multiply charged particles passed by the DMA, complicated analysis for flames with $\phi \geq 4$. Therefore the results presented here are all for fractal soot particles produced at $\phi < 4$.

TABLE 2
Fractional composition by mass of uncoated soot particles

Fuel Equivalence Ratio (ϕ)	BC Mass Fraction ($\pm$ 0.10)	PAH Mass Fraction ($\pm$ 0.10)	AL Mass Fraction ($\pm$ 0.10)
2.3 (fractal)	0.90	0.05	0.05
2.8 (fractal)	0.85	0.10	0.05
3.5 (fractal)	0.75	0.20	0.05
5.0 (near-spherical)	0.60	0.35	0.05

At each ϕ, particles were size-selected by the DMA (see Figure 1) over a range of mobility diameters[2] from 100 nm to 460 nm. The morphology and composition of the particles depend on both ϕ and d_m. The soot particles consist of BC, polycyclic aromatic hydrocarbons (PAH), and aliphatic hydrocarbons (AL). The fractional composition as measured by the AMS-SMPS is shown in Table 2. As shown in the table, the mass fraction of BC is ~90% for particles produced in the flame at $\phi = 2.3$ and decreases to ~75% for $\phi = 3.5$. This change in composition is due to reduced oxygen (less complete combustion) and therefore more PAH compounds formed that condense on the particles (Slowik et al. 2004). The fractional composition depends only on ϕ and is independent of particle size.

Two quantities are used here to describe the particle morphology: the fractal dimension (D_f) and the dynamic shape factor (χ). For $\phi < 4$, D_f is constant and found to be 1.7 ± 0.1, indicating that the particles are fractal. The dynamic shape factor (χ) is defined as the ratio of the drag on a particle to the drag on a sphere of equal volume to the particle. For a sphere, $\chi = 1$, and for non-spherical particles, generally $\chi > 1$. For the fractal soot particles studied here, χ increases with increasing d_m and decreases with increasing ϕ. The inverse relationship between χ and ϕ is due to increased PAH condensation on the soot particles at higher ϕ (see Table 2) which perhaps smoothes over the surface structure of the particles (Slowik et al. 2004). In this study, observed values of χ range from 1.3 ($\phi = 2.8$, $d_m = 100$ nm) to 3.6 ($\phi = 2.3$, $d_m = 460$ nm).

To confirm the soot characterization provided by the AMS-SMPS, Scanning Electron Microscope (SEM) images of the soot were obtained. Particles were sampled on Nucleopore clear

[2]The complete set of selected d_m values is as follows: Uncoated soot: at $\phi = 2.3$, $d_m \sim$ 185, 250, 285, 320, 460; at $\phi = 2.8$, $d_m \sim$ 110, 175, 190, 220, 285, 340, 345, 420, 460; at $\phi = 3.5$, $d_m \sim$ 170, 220, 245, 260, 330, 345, 460; at $\phi = 5.0$, $d_m \sim$ 160, 210, 270, 330, 345; at $\phi =$ 6.0, $d_m \sim$ 160, 335. For thin OA, thin AN, and thick AN coatings: at $\phi = 2.3$, 2.8, and 3.5, $d_m \sim$180, 240, 345; at $\phi = 5.0$, $d_m \sim$ 345. For thick OA coatings: at $\phi = 2.3$, 2.8, 3.5, and 5.0, $d_m \sim$230, 470.

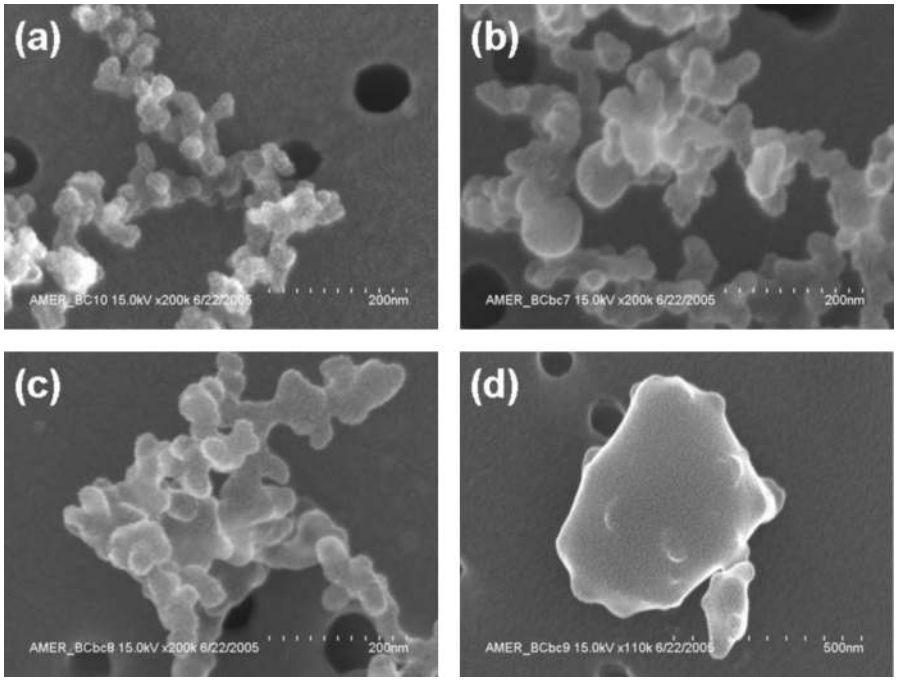

FIG. 3. Scanning electron microscope (SEM) images of soot at four different equivalence ratios: $\phi = 2.3$ (a), $\phi = 2.8$ (b), $\phi = 3.5$ (c), and $\phi = 5.0$ (d).

polycarbonate 13-mm diameter filters mounted in Costar Pop-Top Membrane holders. The filter samples were kept in refrigerated storage. The samples were later coated with a 1 nm-thick layer of platinum to prevent particle charging during SEM analysis. The coated filters were analyzed with a Hitachi Field Emission Scanning Electron Microscope Model S-4700 (accelerating voltage: up to 30 kV, magnification: 50 X to $\sim$ 500,000 X) and a Hitachi Field Emission Scanning Electron Microscope Model S-4800 (accelerating voltage: up to 30kV, magnification: 50 X to $\sim$ 700,000 X).

For each set of experimental conditions, approximately 200 particles were analyzed by SEM for particle shape, fractal dimension, agglomerate size distribution, and monomer size distribution. Particle mass was also estimated, though this measurement may be distorted due to evaporation of non-refractory organics in the SEM. Only a representative sample of the SEM data will be shown here.

The particle morphology described by the AMS-SMPS is also observed in the SEM micrographs shown in Figure 3. This figure shows SEM pictures of soot particles produced at four different equivalence ratios ($\phi = 2.3$, 2.8, 3.5, and 5.0). All particles have $d_m \sim 460$ nm, and in Figures 3a–3c, the AMS-SMPS measurements yield $D_f = 1.7 \pm 0.1$. In Figure 3a ($\phi = 2.3$), $\chi = 3.6$; in Figure 3b ($\phi = 2.8$), $\chi = 3.2$; and in Figure 3c ($\phi = 3.5$), $\chi = 2.5$. It is evident from these pictures that the soot particles produced at $\phi < 4$ are fractal aggregates composed of agglomerated BC spherules. Depending on the flame conditions, typical spherules are 20–60 nm in diameter. For fractal soot of $d_m = 200$ nm produced at $\phi = 2.8$, the number of spherules is on the order of 200. For fuel ratios greater than $\phi > 4$, near-spherical soot particles are produced such as shown in Figure 3d.

The morphology (that is, the size, number, and arrangement of the primary spherules) of soot particles produced in this study has been shown to be similar to that of particles produced by diesel engines at the tailpipe (Park et al. 2004; Slowik et al. 2004). However, the chemical composition of the non-refractory component is different. The non-refractory composition of the laboratory-generated particles consists primarily of PAH compounds, while the diesel-generated particles contain mostly unburnt fuel and lubricating oils. The refractory component (black carbon) of the laboratory soot has not been completely characterized but is expected to be similar to that of diesel soot. This expectation is supported by index of refraction measurements performed on soot produced in a premixed propane/O_2 flame to values for ambient soot. A value of $1.77 + 0.63i$ was obtained for the premixed flame (Chang and Charalampopoulos 1990). Both the real and imaginary parts of this value are in the same range as the value of $1.68 + 0.56i$ obtained for diesel soot (Marley et al. 2001) and the suggested range of values for atmospheric light-absorbing carbon ($1.75 + 0.63i$ to $1.95 + 0.79i$) (Bond and Bergstrom 2006).

Coated Particles

Coating experiments were performed at $\phi = 2.3$, 2.8, 3.5, and 5.0. However, as was pointed out for uncoated soot, in the present experiment at $\phi = 5.0$ both fractal and near-spherical particles are produced. Therefore, we present coating experiments only for $\phi < 5.0$ where the coating experiments can be unambiguously interpreted.

For the non-spherical particles in this study, there is no single parameter which can be used unambiguously to express coating thickness. We measure the total volume (obtained via mass and density) of the material deposited on each particle. (This is obtained from AMS-SMPS data by solving Equations [1–3] for the coated particle and comparing it to the values for the uncoated particle.) This deposited volume is then converted to a change in the volume equivalent radius (Δr_{ve}) (r_{ve} defined in terms of volume as volume $= 4\pi r_{ve}^3/3$), obtained from the difference between the volume of the coated particle and the volume of the uncoated particle. This parameter is the thickness of the deposited layer as if this deposition were placed on a sphere with the same volume as the uncoated particle. Clearly, for non-spherical particles, the parameter Δr_{ve} is not the thickness of the coating. However, if the morphology of the particle is known, Δr_{ve} can be related to the actual coating as described in the next paragraph. The Δr_{ve} representation in itself does not take into account the specific morphology of the particles nor any changes in the morphology resulting from the deposition. The reported uncertainty for Δr_{ve} is one standard deviation of the measured values for a given set of experimental conditions.

If the morphology of the fractal soot particle is known, Δr_{ve} can be used to estimate the lower limit of the coating thickness on the particle as follows. The morphology information provides the size and number of spherules in the uncoated particle (Slowik et al. 2007). We assume that each spherule composing the fractal particle is fully exposed to the gas phase and is evenly coated. The estimated coating thickness is then $\Delta r_{ve} * 4\pi r_{ve}^2$/(particle surface area). This expression yields only the lower limit of the coating thickness because in reality the spherules contact each other and are therefore not completely coated. To illustrate such a calculation, consider a particle produced by a flame at $\phi = 2.1$ with $d_m = 310$ nm. As shown in Slowik et al. (2007), such a particle consists of ~900 spherules of ~15 nm, yielding a ratio of $4\pi r_{ve}^2$/(particle surface area) ~1/11. At $\phi = 3.5$ with $d_m =$ 135 nm, lower limit of the surface area ratio is 1/1.5.

The organic coatings on aerosols affect the particle shape, fractality, and in some cases even the internal particle morphology. Detailed studies of these effects have been performed and are described in Slowik et al. (2007). In the present study, we are concerned only with the effect of coatings on the detection of BC by the instruments involved in this inter-comparison. Coating thicknesses in two ranges were studied for each type of coating material (oleic acid and anthracene). The thickness of the coating was set by the reservoir temperature and was measured by the AMS-SMPS instrument. For oleic acid, at the reservoir temperature of 80°C, the coating produced resulted in $\Delta r_{ve} =$ 10 nm ± 5 nm, and at 90°C the coating resulted in $\Delta r_{ve} = 50$ nm ± 10 nm. For anthracene, at the reservoir temperature of 70°C, the coating resulted in $\Delta r_{ve} = 7$ nm ± 5 nm and at 80°C, the coating resulted in $\Delta r_{ve} = 60$ nm ± 10 nm.

The AMS-SMPS measurements show that both organic coatings decreased the dynamic shape factor (χ) towards a more spherical configuration. Coating experiments were conducted with particles having the initial χ in the range of 1.6–3.6. The thin coatings decreased χ to 1.3–3.0, respectively. The thicker coatings produced a further decrease in χ to 1.1–1.8, respectively. Although the coatings changed the particle dynamic shape factor, the fractal dimension remained unaltered at the initial value of 1.7 ± 0.1 for all coating thicknesses ($\Delta r_{ve} =$ 10 to 60 nm). We interpret these results to mean that the coating follows the original shape of the particle. That is, the coating does not bring about a significant merging of individual spherules. The results of coating experiments performed by Saathoff et al. (2003a, b) are somewhat different. They observed that in the process of coating, the particles remained fractal however the fractal dimension did increase from 1.9 to 2.1. Saathoff et al. attribute the change in fractal dimension to coating-induced compaction of the aggregates. Such restructuring could be hindered in the present study by the presence of flame-generated solid PAH compounds on the soot particles (Slowik et al. 2007).

EXPERIMENTAL RESULTS

The results of these studies will be divided into two categories: (1) results obtained with uncoated soot and GC spheres, and (2) results obtained with soot particles coated with oleic acid and anthracene.

The BC measurement made by the AMS-SMPS is the refractory mass per particle and the BC measurement made by the SP2 is the incandescent mass per particle. On the other hand, the measurement made by the MAAP and PAS is the absorption coefficient of the aerosol ensemble in the optical path sampled by each instrument (B_{abs}). The determination of absorbing mass from the MAAP and PAS instruments relies on an additional calibration factor that relates optical absorption to BC content (obtained by comparison to a thermal method; see instrument descriptions). This conversion is obtained via a wavelength-dependent mass-specific absorption coefficient, σ_{abs}. Because of this distinct grouping, we begin the inter-comparison with separate comparisons of the AMS-SMPS to SP2 (in terms of the incandescent and refractory mass/particle) and MAAP to PAS (in terms of B_{abs}). The additional measurement of number concentration by the CPC then allows us to convert the MAAP and PAS readings to an averaged optically-absorbing mass per particle and to compare these instruments to the AMS-SMPS.

GC Spheres and Uncoated Soot

Comparison of AMS-SMPS to SP2

Under optimal experimental conditions, the size-selecting DMA provides a monodisperse particle size distribution. The SMPS identifies the mobility diameter of particles entering the AMS to within ±10 nm. The AMS yields the average d_{va} and non-refractory composition of the particle ensemble at the selected mobility diameter. In the SP2, the incandescence signal is measured for each individual particle.

The experiment is complicated by the presence of more than one particle mode passed by the size-selecting DMA(s). Both

the AMS-SMPS and SP2 are capable of distinguishing between individual particle modes. However, the separation of the higher modes in the SP2 instrument is often less clear. Therefore, to reduce ambiguity, only the particle mode with the smallest d_m is considered in the comparison of these two instruments.

Two SP2 instruments (operated by NOAA and DMT) were utilized in this study. In Figure 4, we present inter-comparison data for the commercial GC spheres. The GC spheres were used to calibrate the SP2 instruments, because the mass of these particles can be unambiguously calculated from the measurement of d_{va} and d_m provided by the AMS-SMPS. For both instruments, the incandescence peak height was linearly related to particle mass. In the NOAA instrument, mass calibration is 0.155 fg/incandescence unit. In the DMT instrument, the calibration is 0.1106 fg/incandescence unit. For each instrument, its own calibration was applied to each data point to yield the incandescent mass.

The GC mass/particle as measured by both SP2 instruments using this calibration is plotted vs. the AMS-SMPS measurement. In all inter-comparison figures, the dashed 1:1 line is shown to aid the eye. The slope of a linear fit forced through zero is 1.0 ± 0.1 for the NOAA SP2, and 1.0 ± 0.2 for the DMT SP2. The reported errors are one standard deviation of the points to the best fit line; that is, 68% of the points fall between the lines designated by the slope and errors. The slope and errors determined in this way will be reported for each inter-comparison plot presented. The slope of a line not forced through zero differs from the reported values typically by less than 10%. Note that the 1:1 agreement evident in Figure 4 is due to the fact that this data set was used to calibrate the SP2 instruments. Deviation from the 1:1 line indicates potential magnitude of experimental variability.

The SP2 measurements of incandescent mass/particle for uncoated soot are plotted vs. the AMS-SMPS measurements for the NOAA and DMT instruments in Figures 5a and 5b, respectively. Separate symbols are used to represent different equivalence ratios (ϕ). Both SP2 instruments agree with the AMS-SMPS to within 15% for uncoated fractal soot. However, the NOAA instrument tends to overestimate the BC content, particularly at relatively high BC mass, while the DMT instrument underestimates it. Although the data from the DMT instrument appear to be offset from the 1:1 line, subsequent experiments with coated soot indicate that the data in fact project to a zero-zero intercept. We also note that the response of the SP2 instruments relative to the AMS-SMPS is independent of ϕ.

We do not know the reason for the 15% difference in response of the NOAA and DMT instruments, but suspect that it is likely

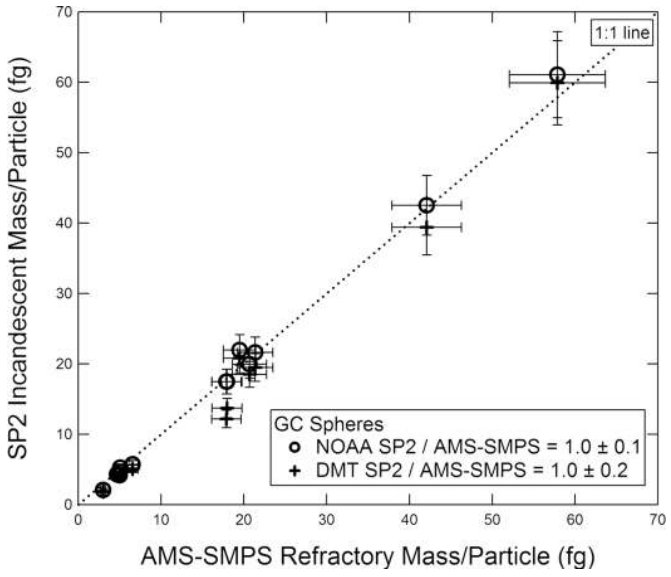

FIG. 4. Incandescent mass per particle measured by the SP2 instruments vs. refractory mass per particle measured by the AMS-SMPS for commercial GC spheres. The NOAA and DMT instruments are represented by different symbols.

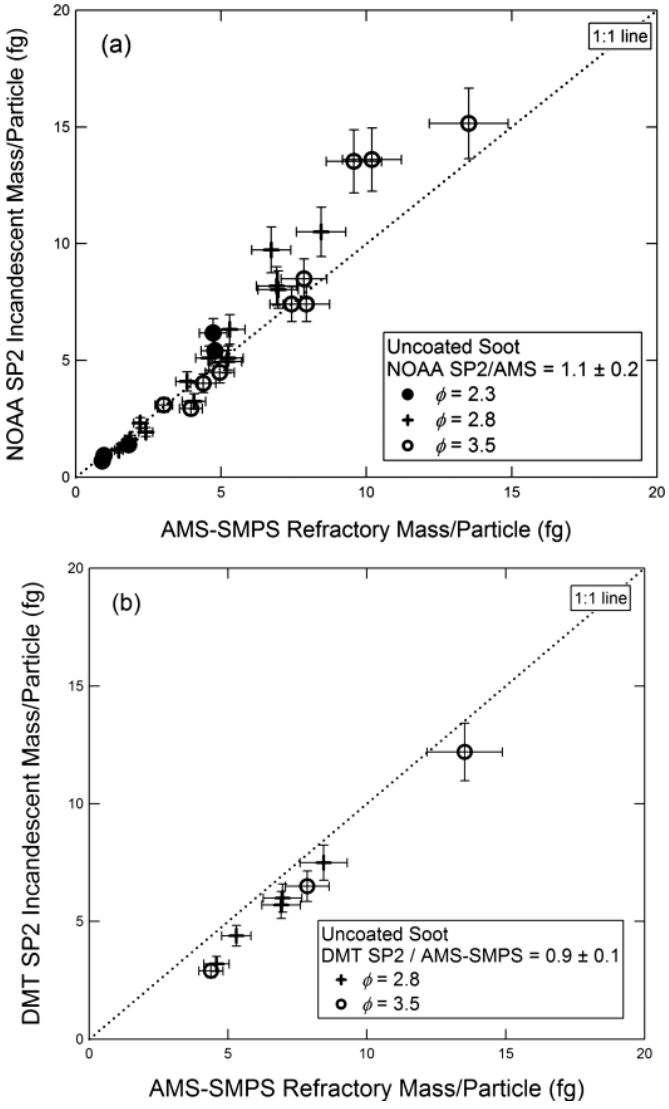

FIG. 5. Incandescent mass per fractal soot particle measured by (a) the NOAA SP2 and (b) the DMT SP2, both plotted vs. refractory mass per particle measured by the AMS-SMPS. Fuel equivalence ratios are as shown in the figure.

due to the following factors. The two instruments utilized lasers set at different powers and were aligned differently. This may result in output differences as large as 10% due to the location of particle incandescence. (The response across the face of the APD detector is not fully linear.) Further, reflections from the DMT filters, which are mounted differently in the two instruments, could cause shifts in response as large as 10%.

Comparison of MAAP to PAS

The MAAP measures B_{abs} at 670 nm, and the PAS measures B_{abs} at 870 nm. To compare the instruments, the MAAP B_{abs} measurement is converted to 870 nm assuming an inverse wavelength relationship, which has been observed for BC-containing particles in previous studies (i.e., $B_{abs} = C\lambda^{-1}$, where C is a dimensionless proportionality constant) (Bruce et al. 1991; Horvath et al. 1997; Bergstrom et al. 2002; Sheridan et al. 2005).

Figure 6 is a plot of the MAAP B_{abs} versus the PAS B_{abs} for GC spheres. These instruments were calibrated in other experiments as discussed in the Experimental section. The GC spheres were not used as a calibrating standard. The slope of the best fit lines (forced through zero) is 0.9 ± 0.3 for GC spheres. While the two instruments agree within experimental error, the MAAP reading is slightly lower relative to the PAS instrument ($\sim$7%).

Figure 7 is a plot of the MAAP B_{abs} vs. the PAS B_{abs} for uncoated fractal soot. The fuel equivalence ratios used in the soot generation are shown in the figure by different symbols. The readings of the two instruments agree within experimental scatter. However, the reading of the MAAP in this case is higher than the PAS by about 20% (slope $= 1.2 \pm 0.2$). The figure shows that, as was the case with the SP2/AMS-SMPS comparison, the relative response of the two instruments is independent of the equivalence ratio.

While the aerosol absorption coefficient (B_{abs}) is the primary measurement of these two instruments, B_{abs} can be converted

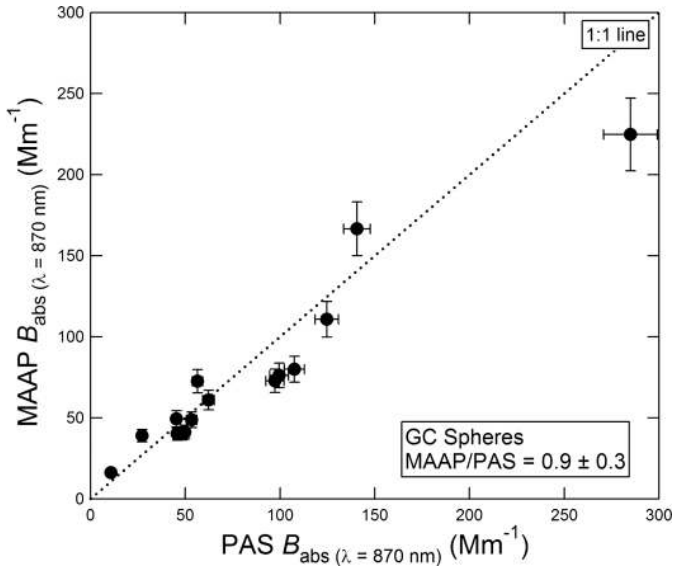

FIG. 6. Comparison of aerosol absorption coefficients (B_{abs}) measured by the MAAP vs. PAS for commercial GC spheres.

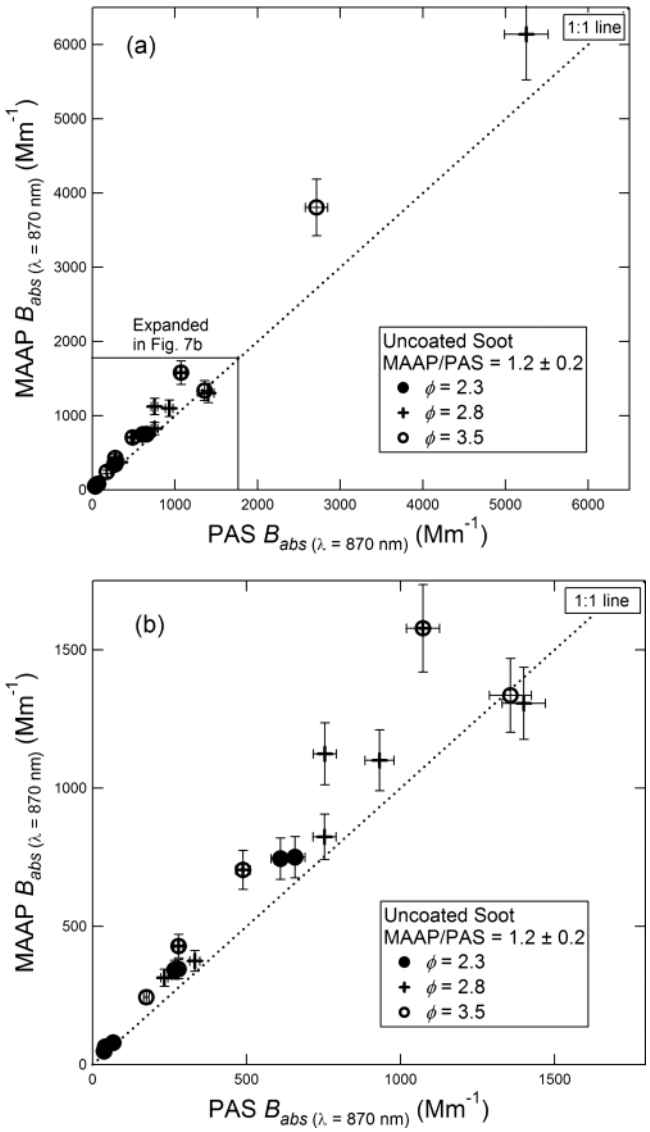

FIG. 7. Aerosol absorption coefficient (B_{abs}) for fractal soot measured by the MAAP plotted vs. the PAS. The data for lower values of B_{abs} is expanded in (b). Fuel equivalence ratios are as shown in the figure.

to optically-absorbing mass per unit volume and in this way the MAAP and PAS instruments can be compared to the SP2 and AMS-SMPS instruments. This conversion uses the mass-specific absorption coefficient (σ_{abs}) as stated in the Description of Instruments section. The PAS uses a $\sigma_{abs-PAS}$ of 6.2 m^2 g^{-1}at 870 nm, while the MAAP uses a $\sigma_{abs-MAAP}$ of 5.1 m^{2}g^{-1} at 870 nm (converted from its value at the instrument wavelength of 670 nm via inverse wavelength dependence). As will be discussed later, the difference in the two σ_{abs} values may be due to the accuracy of instrument calibration and/or the type of particles used to calibrate the instrument. The optically-absorbing mass measured by the MAAP and PAS is converted to mass per particle via measurement of the particle concentration with a CPC (see apparatus diagram in Figure 1). This mass/particle

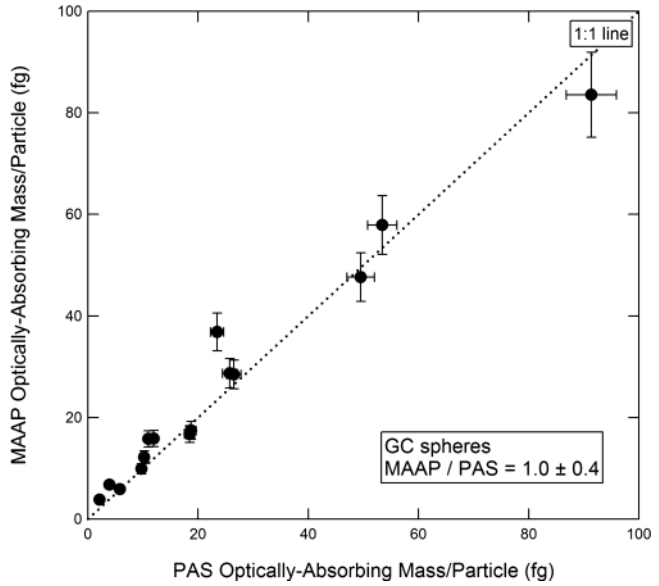

FIG. 8. Optically absorbing mass per particle measured by the MAAP vs. PAS for commercial GC spheres.

measurement is the average value for all the particles in the optical path of the MAAP and PAS instruments. That is, the entire particle ensemble passed by the size-selecting DMA is included in the calculation of the optically-absorbing mass/particle. In Figures 8 and 9, the per particle comparisons are made for the MAAP and PAS instruments for GC spheres and uncoated soot, respectively. These two figures parallel the comparison made in terms of B_{abs} in Figures 6 and 7. This per particle presentation made in Figures 8 and 9 will make it possible to inter-compare all four instruments, as discussed in the next section.

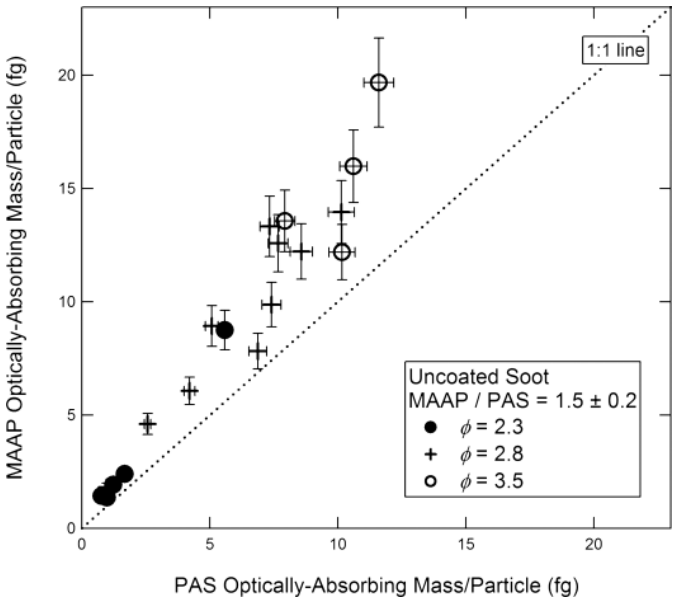

FIG. 9. Optically absorbing mass per fractal soot particle measured by the MAAP vs. the PAS. Fuel equivalence ratios are as shown in the figure.

The comparisons shown in Figures 8 and 9 on a mass/particle basis do not yield the same result as those based on the absorption coefficient B_{abs} (shown in Figures 6 and 7) because the mass-specific absorption coefficients (σ_{abs}) are different for the two instruments. Consequently, the slopes and deviations in Figures 8 and 9 are larger than in Figures 6 and 7. The slope in Figure 8 is 1.0 ± 0.4 compared to 0.9 ± 0.3 in Figure 6, and 1.5 ± 0.2 in Figure 9 compared to 1.2 ± 0.2 in Figure 7 for uncoated soot.

The relative response of the two instruments is different for GC spheres and uncoated soot. Relative to the PAS, the MAAP measures a smaller absorbance for GC spheres and a larger absorbance for fractal soot. Based only on Figures 6–9, it is not evident whether the difference is due to the response of the MAAP, PAS, or both. However, the results presented in the following section suggest that the difference in the response is due to the higher reading for uncoated fractal soot obtained from the MAAP instrument. As will be explained in the Discussion section, the difference between the results for uncoated soot and the GC spheres is due to the dependence of σ_{abs} on particle size for the GC spheres.

Inter-Comparison of the Four Instruments

General Considerations. The inter-comparison of the four instruments is complicated by the presence of multiple particle modes passed by the size-selecting DMA. The MAAP and PAS measure properties of the particle ensemble, the SP2 measures the properties of individual particles, and the AMS-SMPS yields an average BC mass for particles belonging to each size mode. Under ideal conditions, the SP2 measurements of BC mass on a single particle basis can be converted to an ensemble average. However, the precision of the SP2 single particle measurement is inversely proportional to the measured particle mass and under some experimental conditions the modes at higher charges (larger particles) overlap and are not distinguishable from each other. Only the mode containing the singly charged, smaller particles is clearly resolved under the full range of experimental conditions. The AMS-SMPS, on the other hand, can resolve all the significant particle modes and therefore this instrument could provide both an ensemble average and individual particle mobility diameter mode readings. Therefore the AMS-SMPS is used as the reference for inter-comparing all four instruments. Note that the selection of the AMS-SMPS as the reference instrument should not be interpreted as an *a priori* claim on the absolute accuracy of its measurement.

In the comparison of instrument response to coated and uncoated particles presented below, the experiments were performed sequentially, which is an experimental necessity. This procedure is justified by repeated measurements that show the soot particles produced by the flame under a set of flow conditions to be fully reproducible. From day to day, the refractory mass measured by the AMS-SMPS for a given d_m and ϕ varies by less than $\pm$ 5%, which is within the measurement error of the instrument.

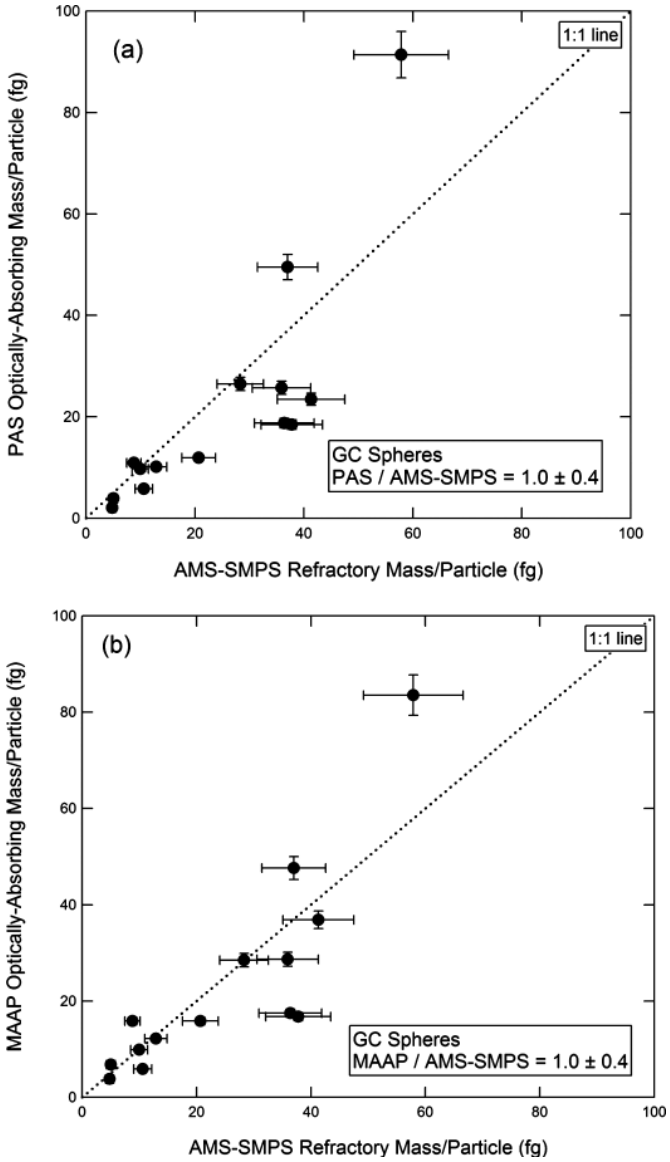

FIG. 10. Optically absorbing mass per particle measured by the PAS (a) and MAAP (b) vs. refractory mass per particle measured by the AMS-SMPS for commercial GC spheres.

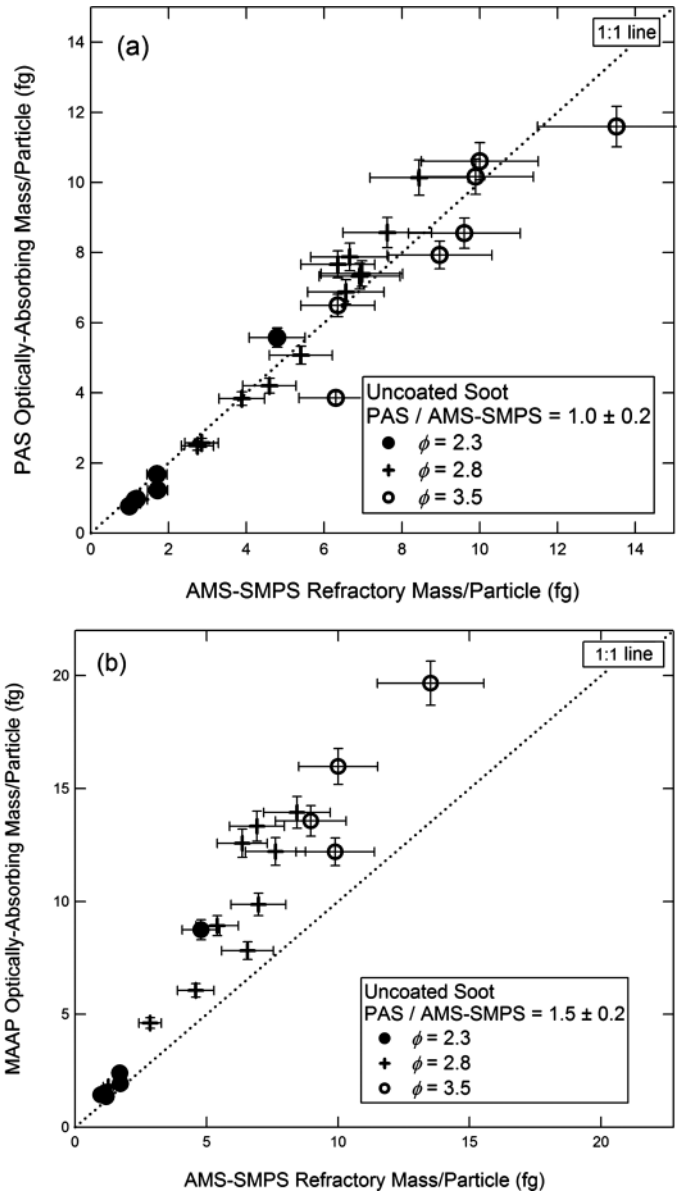

FIG. 11. Optically absorbing mass per fractal soot particle measured by (a) the PAS and (b) the MAAP, both plotted vs. the refractory mass per particle measured by the AMS-SMPS. Fuel equivalence ratios are as shown in the figure.

Results of Instrument Inter-Comparison. In Figure 10, the GC mass/particle for commercial GC spheres is plotted for the PAS (10a) and the MAAP (10b), both referenced to the AMS-SMPS. The slope of the best fit line in Figure 10a is 1.0 ± 0.4 for the PAS, and in Figure 10b the slope is 1.0 ± 0.4 for the MAAP. The corresponding plots for uncoated soot are shown in Figures 11a and b. The slope of the best fit line in Figure 11a is 1.0 ± 0.2 for the PAS, and in Figure 11b is 1.5 ± 0.2 for the MAAP. The per particle plots comparing the SP2 instruments to the AMS-SMPS are shown in Figures 4 and 5. These four figures display the full inter-comparison of GC spheres and uncoated soot.

The full inter-comparison is presented as a bar graph in Figure 12. In Figure 12, the data from the two SP2 instruments have been combined and the scatter recalculated. The error bars for the other instruments in Figure 12 are the ones shown in the individual comparison plots.

The scatter in the data comparing the MAAP and PAS to the AMS-SMPS is greater for BC spheres than for uncoated soot. The increase in the scatter is most likely due to the complications in extracting the data required to calculate the ensemble refractory mass from the AMS-SMPS. This is mainly due to the fact that the polydisperse distribution of the GC spheres is weighted towards larger particles. This presents two difficulties.

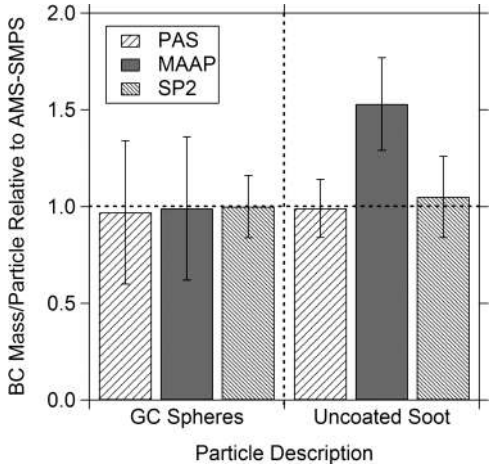

FIG. 12. Summary of instrument inter-comparison for GC spheres and uncoated soot. Readings are normalized to the AMS-SMPS measurements.

First, when the distribution is weighted towards larger particles, the number of multiply charged particles in the larger size modes increases, making it more difficult to distinguish the individual modes. Second, the larger modes approach the instrument cutoff for larger particles, reducing the accuracy of number determination in this range.

As shown in Figure 12, for uncoated soot, the agreement between the AMS-SMPS, PAS, and SP2 is within ∼10%, while the measurement obtained from the MAAP data is ∼1.5 times higher. In discussing the uncoated soot measurements obtained with the MAAP and PAS alone, we pointed out in the previous section that it was not clear from the results based on just the two instruments whether the MAAP was over-indicating or whether the PAS was under-indicating the BC content of uncoated soot. Comparing the instruments with respect to the AMS-SMPS as is done in Figure 12 resolves this question and shows that the MAAP reading is higher for the fractal soot. This result will be further addressed in the Discussion section.

Coated Soot Particles

The purpose of the coating experiments is to determine whether an organic coating on a particle affects the measurement of BC by the different instruments. A partial answer to this question can already be obtained by considering the results obtained with uncoated soot particles described in the previous section. These particles consist of aggregated BC spherules mixed with flame-generated organics (mostly PAHs). As shown in Table 2, depending on the equivalence ratio, the non-refractory organic component constitutes 5% to 20% of the particle mass. If we assume that the flame-generated organics coat the aggregate, then such a coating thickness would result in Δr_{ve} of 1 nm to 15 nm, increasing with ϕ. The BC reading of each of the four instruments is independent of the equivalence ratio, implying that organic coatings on the order of ∼10 nm do not affect the BC readings. The coating experiments explicitly explore this issue for thicker coatings.

The particles were coated with oleic acid and anthracene. For each organic molecule, two coating thicknesses were studied. For oleic acid, coatings with Δr_{ve} of 10 nm ± 5 nm and 50 nm ± 10 nm and for anthracene, coatings with Δr_{ve} of 7 nm ± 5 nm and 60 nm ± 10 nm were studied. The thinner coatings are approximately the same thickness as those generated by the flame at $\phi = 3.5$. The coating experiments were performed at ϕ ranging from 2.3–3.5.

Measurements over the full range of fractal aerosol sizes and flame conditions showed that the thin experimentally deposited coatings on soot particles both of oleic acid and anthracene do not affect the BC measurements obtained from any of the instruments. These measurements are not presented here.

On the other hand, the thicker organic coatings in some cases had a pronounced effect on BC measurements and the results are presented here. For each instrument, we will present plots of the BC mass/particle of coated vs. uncoated particles. Plots for the AMS-SMPS, SP2, MAAP, and PAS are shown respectively in Figures 13–16. In Figure 14, the SP2 measurements of anthracene-coated particles include data from both the DMT and NOAA instruments, while for the oleic acid coatings, only data from the NOAA instrument are available. The slopes and standard deviations of the data points are shown in the figures. Within experimental error, there is no difference in the measurements of anthracene-coated soot particles by the two SP2 instruments.

The readings of the AMS-SMPS and SP2 (Figures 13 and 14) are within experimental error of the 1:1 line, indicating that the coating does not significantly affect the BC reading of these instruments. The reading of the MAAP (Figure 15) is within experimental error of the 1:1 line, although the slope of the best fit line is ∼20% higher. However, as shown in Figure 16, the

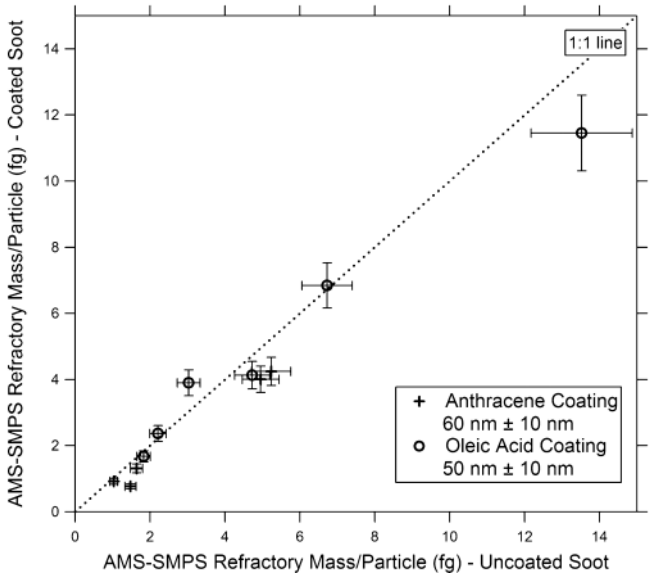

FIG. 13. AMS-SMPS measurement of refractory mass/particle for coated vs. uncoated soot. Coating materials and Δr_{ve} are as shown in the figure.

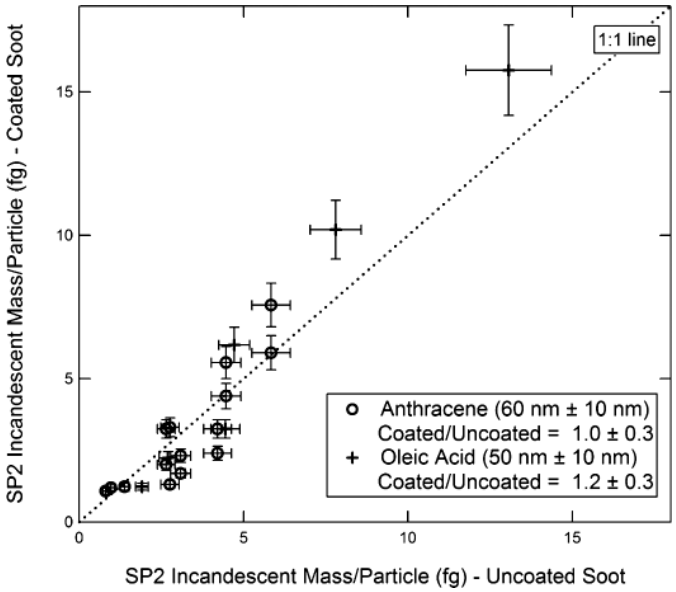

FIG. 14. SP2 measurement of incandescent mass/particle for coated vs. uncoated soot. Coating materials and Δr_{ve} are as shown in the figure. The anthracene data are obtained both from the DMT and NOAA instruments. Oleic acid data are available only from the NOAA instrument.

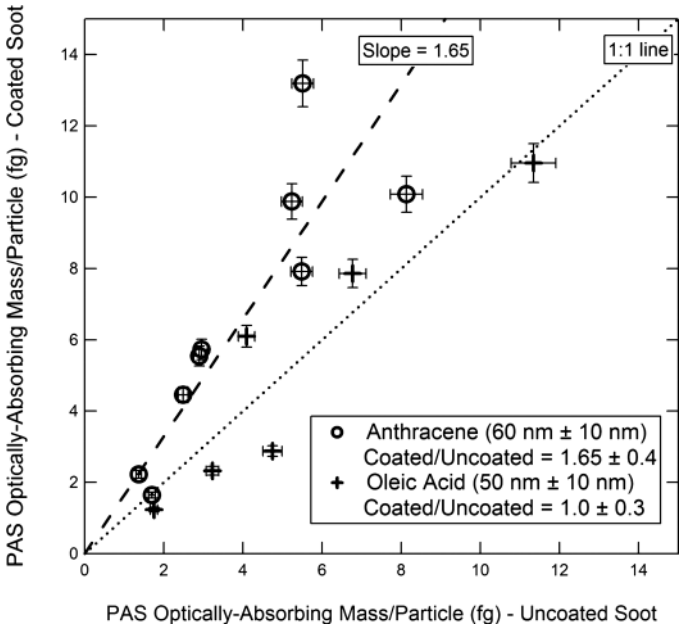

FIG. 16. PAS measurement of optically absorbing mass/particle for coated vs. uncoated soot. Coating materials and Δr_{ve} are as shown in the figure. The dashed line is the best linear fit (slope 1.65) to the anthracene-coated particles.

60 nm anthracene coating increases the BC reading of the PAS instrument by about 65%, which is outside the scatter in the data points.

The inter-comparison results for both thickly-coated and uncoated particles are summarized in Table 3 (the thin coatings did not affect the measurements of BC by any of the instruments). The BC reading of each instrument relative to the AMS-SMPS is given for GC spheres, uncoated soot, and the thick oleic acid and anthracene coatings.

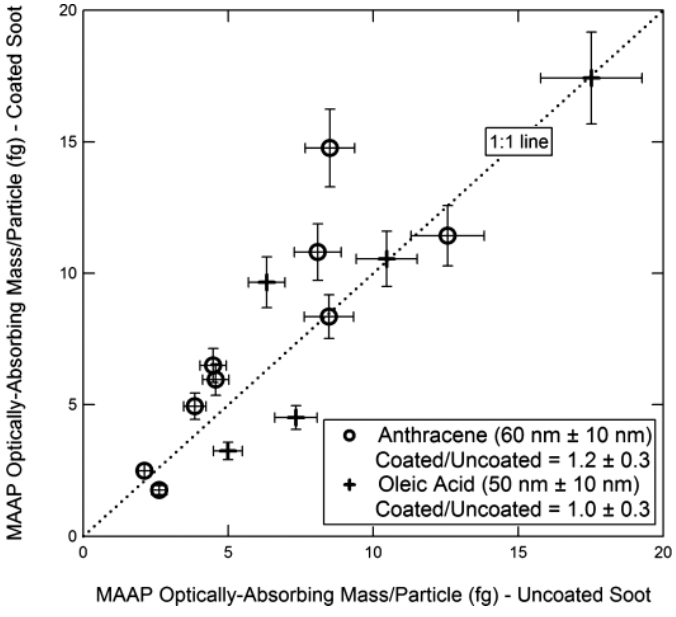

FIG. 15. MAAP measurement of optically absorbing mass/particle for coated vs. uncoated soot. Coating materials and Δr_{ve} are as shown in the figure.

DISCUSSION

The present study compares the performance of four types of instruments with respect to their measurement of BC content of fractal soot aerosols produced in an ethylene/O_2 flame. At the outset of this study, the interpretation of the measurements provided by each instrument involved certain assumptions. An important outcome of the experiments was the testing of the assumptions inherent in the instrument operation. The following discussion will focus on describing the extent to which these assumptions were clarified. The results obtained with each technique will be evaluated.

AMS-SMPS

In the initial analysis of the results obtained with the AMS-SMPS technique (Slowik et al. 2004; DeCarlo et al. 2004), several assumptions were made about the nature of the aerosol particles. Specifically, the particles were assumed to have no internal voids, the PAH, aliphatic, and BC components were assumed to be immiscible, and the dynamic shape factor was assumed to be the same in the free-molecular and continuum regimes. Further, it was assumed that the non-refractory component of the particles does not pyrolyze at the AMS vaporizer and that the coatings do not evaporate in the aerodynamic lens. The assumption that the coatings do not evaporate in the aerodynamic lens has been verified for oleic acid by comparing the d_m and d_{va} of pure oleic acid particles, which agree within the measurement limit ($\sim$2%) after accounting for the particle density.

TABLE 3
BC mass per particle measured by the MAAP, PAS, and SP2 relative to the AMS-SMPS measurement for GC spheres, uncoated soot, and thick coatings of oleic acid and anthracene. Thin coatings of oleic acid and anthracene had no effect on the instrument readings.

Instrument	GC Spheres	Uncoated Soot	Oleic Acid Coating (50 nm ± 10 nm)	Anthracene Coating (60 nm ± 10 nm)
MAAP/AMS-SMPS	1.0 ± 0.4	1.5 ± 0.2	1.5 ± 0.5	1.8 ± 0.5
PAS/AMS-SMPS	1.0 ± 0.4	1.0 ± 0.2	1.0 ± 0.3	1.6 ± 0.4
SP2/AMS-SMPS	1.0 ± 0.2	1.1 ± 0.2	1.3 ± 0.4	1.0 ± 0.3

The AMS-SMPS measurement of refractory mass for uncoated soot agrees within experimental error with the SP2 measurement of incandescent mass and the PAS measurement of optically-absorbing mass. We note that due to the chemical nature of the particles used in this experiment, these masses are expected to be similar. Therefore, the agreement between instrument readings expressed as a mass increases one's confidence in the measurements provided by these instruments. In the case of the AMS-SMPS, the agreement suggests that the assumptions described above do not introduce significant error into the AMS-SMPS measurement (because these assumptions are not involved in the measurements obtained with the SP2 and PAS). Further, because the calculation of refractory mass by the AMS-SMPS is tied to particle morphology (see Equations [1–3]), the agreement between instruments likewise supports the values of the shape properties provided by the AMS-SMPS.

SP2

Experiments with uncoated soot particles and GC spheres confirms a key assumption in the interpretation of the SP2 data. That is, that the peak of the incandescence signal is linearly proportional to BC mass (rather than, for example, the surface area of the particles). Further, for a given mass, the incandescent signal is independent of particle morphology. That is, the relationship between the SP2 measurement of incandescent mass and the AMS-SMPS measurement of refractory mass is the same for fractal soot and for the GC spheres (see Figures 4 and 5). This suggests that the GC spheres are appropriate as a calibration standard for the SP2.

As shown in Figure 14, the BC reading provided by the SP2 is unaffected by the organic coatings used in these experiments. This suggests that the organic coatings are not charred by the impinging laser light. Rather, they evaporate in the process of laser-induced heating of the particle. Direct evidence of evaporation is obtained from a time-resolved analysis of the SP2 signal. The SP2 detects both a scattered light signal (at the wavelength of the laser) and a incandescent light signal. For the coated particles, the SP2 recorded first a signal corresponding to scattered light from the coated particle followed by the incandescent signal. The scattered light signal decayed on a timescale of approximately 10 μs. This suggests that, in the process of particle heating, first the non-refractory components evaporate, and then as the temperature rises, BC incandescence is observed. The amplitude of the scattered light signal is strongly dependent on coating thickness. The incandescent signal is independent of coating. The time delay between the peak of the scatter signal and the peak of the incandescent signal is observed to increase with coating thickness. In these experiments, only coatings readily volatilized at temperatures up to ~100°C were studied. The effect of less volatile coatings such as $(NH_4)_2SO_4$ remains to be examined.

MAAP and PAS

Uncoated Particles

As shown in Figure 7, the aerosol absorption coefficient (B_{abs}) for uncoated fractal soot is measured to be 1.2 times higher by the MAAP instrument than the PAS. A similar difference between these two instruments was observed during the RAOS study (Petzold et al. 2005). The reason for this difference is not yet understood. While particle orientation may play a role (Fuller et al. 1999), at present this cannot be conclusively demonstrated.

While the MAAP B_{abs} reading is a factor of 1.2 higher than the PAS for fractal soot, the MAAP reading for GC spheres is lower than that of the PAS (0.9 of PAS). To understand these differences, one must examine the dependence of optical absorption cross-section (σ_{abs}) on particle size. For the uncoated fractal soot particles, the particles are small relative to the wavelength because the relevant size parameter is the diameter of the primary spherules (30–40 nm). In this regime, σ_{abs} is nearly independent of particle size. However, in the size range of the GC spheres, (diameter = 165–460 nm) σ_{abs} decreases with increasing particle size. As a result, with respect to optical absorption, the uncoated soot particles are the simpler case. Further, the decrease in σ_{abs} with particle size for the GC spheres is greater for the MAAP than the PAS because the MAAP wavelength is shorter. Thus, the similar absorption measured for GC spheres by the two instruments is fortuitous and cannot be simply interpreted as an agreement in the absorption measurements provided by these two instruments. Rather, the agreement in the case of the GC spheres is due to the GC particle size. This issue is discussed further in Appendix A, where it is shown that the results obtained in this study are consistent with modeling results of Fuller et al. (1999).

The wavelength and diameter dependence of σ_{abs} as discussed above lead to the conclusion that the GC spheres in the diameter range studied here are not suitable standards for optical absorption-based instruments in the visible range.

The dependence of σ_{abs} on particle size may also have implications for absorption-based measurements of atmospheric aerosols. Laboratory experiments have shown that under certain conditions (for example, condensation of organics), the structure of BC fractal aggregates can collapse into a more spherical configuration (Schnaiter et al. 2003; Saathoff et al. 2003b). Such a structural change could transform the particle into a regime where the total BC volume, rather than the individual spherules, determines absorption. In such a case, the optical absorption would decrease and the optical measurement would have to be interpreted in terms of both the wavelength of the probing light and the particle diameter.

As was previously noted in the Description of Instruments section, the σ_{abs} values obtained from prior calibrations for the MAAP and PAS are different (5.1 m^2g^{-1} vs. 6.2 m^2g^{-1} at 870 nm). The difference in these σ_{abs} values may be due to two factors. First, the previously noted (and unexplained) difference between the MAAP and PAS measurements of B_{abs} would lead to a discrepancy in σ_{abs}. Second, bias may be introduced by the use of different types of calibration particles and/or different reference techniques for BC mass measurements during the initial calibration of these instruments. Because the fractal calibration particles are composed of primary particles that are small relative to the instrument wavelength, it is not expected that particle morphology would influence the calibration. However, the chemical composition of the BC material used for the calibration of the two instruments may not be the same. Both calibrations rely on comparison to masses measured via thermal techniques, which were not the same for the two instruments. As we note in the Introduction, different heating/oxidation protocols can lead to significant differences in the amount of BC mass measured. It is known that there is significant variation in the properties of BC-containing particles depending on the particle source (Fuller et al. 1999). The recent review by Bond and Bergstrom (2006), notes that most of the recorded values of σ_{abs} fall in the range 4.0–5.4 m^2g^{-1} at 870 nm (converted from 550 nm), and suggest the use of 4.7 m^2g^{-1} (at 870 nm) as a standard. The agreement in the BC mass measurement between the PAS, SP2, and AMS-SMPS for uncoated soot supports the value for $\sigma_{abs-PAS}$ of 6.2 m^2g^{-1} obtained by prior calibrations. While the $\sigma_{abs-MAAP}$ obtained in prior calibrations was 5.1 m^2g^{-1}, the inter-comparison experiments with uncoated soot suggest that the value of $\sigma_{abs-MAAP}$ should be about 20% higher, that is, 7.7 m^2g^{-1} at 870 nm. (This $\sigma_{abs-MAAP}$ value converts to 10.0 m^2g^{-1} at the instrument wavelength of 670 nm.)

Coated Particles

Our experiments show that the response of the MAAP and PAS is unaffected by a Δr_{ve} ~10 nm organic coating of either oleic acid or anthracene, or by a Δr_{ve} ~50 nm coating of oleic acid. In the comparison of the particles covered with a Δr_{ve} ~60 nm anthracene coating to the uncoated, the MAAP readings were ~20% higher, but still within experimental error of the 1:1 line (see Figure 15). On the other hand, a Δr_{ve} ~60 nm anthracene coating caused a ~65% increase in the PAS BC reading (see Figure 16).

Neither oleic acid nor anthracene is expected to be a significant absorber of light. The increase in the PAS and MAAP optical absorption measurements for anthracene-coated particles and the unchanged absorption for particles coated with oleic acid is perhaps explained by the lensing effect of the coatings. The magnitude of absorption enhancement due to coatings depends primarily on the coating thickness and refractive index of the coating material. The increased absorption due to coatings has been treated theoretically among others by Fuller et al. (1999). Direct comparison of modeling studies to laboratory data, however, is complicated by the non-uniformity and lack of precise knowledge of the coating in the present studies. As stated in the Experimental Results section, for the thick coatings the lower limit for the coating thickness is 5–10 nm and the upper limit is 50–70 nm. Fuller et al. (1999) predict that a 5–10 nm coating of a material with refractive index = 1.53 on a 30 nm BC sphere would increase the optical absorption by ~50%. A 50–70 nm coating of such a material would increase the absorption ~250%. Decreasing the refractive index of the coating material from 1.53 to 1.47 reduces the enhancement in absorption by ~30%. In the present study, the coating materials used have refractive indices of 1.46 (oleic acid) and 1.59 (anthracene). With a linear extrapolation of the Fuller et al. calculation, the absorption enhancement by anthracene coating can be explained by an anthracene coating of about 10 nm. A similar coating thickness of oleic acid would produce an enhancement ~20%, which is not observable within experimental error.

CONCLUSIONS

Inter-comparison studies with well-characterized fractal soot particles showed that for uncoated soot particles, the mass measurements by the AMS-SMPS, SP2, and PAS instruments were in agreement to within 15%, while the MAAP measurement of optically-absorbing mass was higher by ~50%. It is suggested that this discrepancy might be a result of the pre-existing MAAP calibration for conversion of absorption to mass. A 20% difference in the absorption measurements of the PAS and MAAP remains unexplained. The agreement between the SP2, AMS-SMPS, and PAS instruments shows that the SP2 provides a measure of incandescent mass per particle independent of particle morphology. The studies also support the AMS-SMPS technique of determining refractory mass.

Thin organic coatings (~10 nm) did not affect the instrument readings. A thicker (~50 nm) oleic acid coating likewise did not affect the instrument readings. The thicker (~60 nm) anthracene coating did not affect the readings provided by the AMS-SMPS or SP2 instruments but increased the reading of the MAAP

instrument by ∼20% and the reading of the PAS by ∼65%. The difference between the oleic acid and anthracene coatings is attributed to the different refractive indices of the two materials.

While the MAAP absorption reading is a factor of 1.2 higher than the PAS for fractal soot, the MAAP reading for commercial GC spheres is lower than that of the PAS by a factor of 0.9. The result was explained by the fact that the GC spheres are not small relative to the wavelength of light. As a result, GC spheres in the size range studied here are not suitable as calibration standards for optical absorption-based instruments in the visible range. On the other hand, the GC spheres are appropriate as calibration standards for the incandescence-based SP2.

REFERENCES

Allan, J. D., Jimenez, J. L., Coe, H., Bower, K. N., Williams, P. I., and Worsnop, D. R. (2003). Quantitative Sampling Using an Aerodyne Aerosol Mass Spectrometer. Part 1: Techniques of Data Interpretation and Error Analysis, *J. Geophys. Res.-Atmospheres*, 108(D3):4090.

Arnott, W. P., Moosmüller, H., and Rogers, D. F. (1999). Photoacoustic Spectrometer for Measuring Light Absorption by Aerosols: Instrument Description, *Atmos. Environ.* 33:2845–2842.

Arnott, W. P., Moosmüller, H., and Walker, J. W. (2000). Nitrogen Dioxide and Kerosene-Flame Soot Calibration of Photoacoustic Instruments for Measurement of Light Absorption by Aerosols, *Rev. Sci. Instrum.* 71(12):4545–4552.

Arnott, W. P., Hamasha, K., Moosmüller, H., Sheridan, P. J., and Ogren, J. A. (2005a). Towards Aerosol Light-Absorption Measurements with a 7-Wavelength Aethalometer: Evaluation with a Photoacoustic Instrument and 3-Wavelength Nephelometer, *Aerosol Sci. Technol.* 39:17–29.

Arnott, W. P., Zielinska, B., Rogers, C. F., Sagebiel, J., Park, K., Chow, J., Moosmüller, H., Watson, J. G., Kelly, K., Wagner, D., Sarofim, A., Lighty, J., and Palmer, G. (2005b). Evaluation of 1047-nm Photoacoustic Instruments and Photoelectric Aerosol Sensors in Source-Sampling of Black Carbon Aerosol and Particle-Bound PAHs from Gasoline and Diesel Powered Vehicles, *Environ. Sci. Technol.* 39(14):5398–5406.

Baumgardner, D., Kok, G., and Raga, G. (2004). Warming of the Arctic Lower Stratosphere by Light Absorbing Particles, *Geophys. Res. Lett.* 31:L06117.

Bergstrom, R. W., Russell, P. B., and Hignett, P. (2002). Wavelength Dependence of the Absorption of Black Carbon Particles: Predictions and Results from the TARFOX Experiment and Implications for the Aerosol Single Scattering Albedo, *J. Atmos. Sci.* 59:567–577.

Bond, T. C., Anderson, T. L., and Campbell, D. (1999). Calibration and Intercomparison of Filter-Based Measurements of Visible Light Absorption by Aerosols, *Aerosol Sci. Technol.* 30(6):582–600.

Bond, T. C., and Bergstrom, R. W. (2006). Light Absorption by Carbonaceous Particles: An Investigative Review, *Aerosol Sci. Technol.* 40(1):27–67.

Bruce, C. W., Stromberg, T. F., Gurton, K. P., and Mozer, J. B. (1991). Trans-Spectral Absorption and Scattering of Electromagnetic Radiation by Diesel Soot, *Appl. Opt.* 30:1537–1546.

Chakrabarty, R. K., Moosmüller, H., Garro, M. A., Arnott, W. P., Walker, J. W., Susott, R. A., Babbitt, R. E., Wold, C. E., Lincoln, E. N., and Hao, W. M. (2006). Emissions from the Laboratory Combustion of Wildland Fuels: Particle Morphology and Size, *J. Geophys. Res.* **111**, D07204. doi:10.1029/2005jd006659.

Chang, H., and Charalampopoulos, T. T. (1990). Determination of the Wavelength Dependence of Refractive Indices of Flame Soot, *Proc. R. Soc. Lond. A* 430:577–591.

Chow, J. C., Watson, J. G., Pritchett, L. C., Pierson, W. R., Frazier, C. A., and Purcell, R. G. (1993). The DRI Thermal/Optical Reflectance Carbon Analysis System: Description, Evaluation, and Applications in U.S. Air Quality Studies, *Atmos. Environ.* 27A:1185–1201.

Countess, R. J. (1990). Interlaboratory Analysis of Carbonaceous Aerosol Samples, *Aerosol Sci. Technol.* 12:114–121.

Cross, E. S., Slowik, J. G., Davidovits, P., Allan, J. D., Canagaratna, M. R., Lewis, D. K., Jayne, J. T., Worsnop, D. R., and Onasch, T. B. (2007). Laboratory and Ambient Particle Density Determinations Using Light Scatterings in Conjunction with Aerosol Mass Spectroscopy. *Aerosol Sci. Technol.* 41(4). In press.

DeCarlo, P., Slowik, J. G., Worsnop, D. R., Davidovits, P., and Jimenez, J. L. (2004). Particle Morphology and Density Characterization by Combined Mobility and Aerodynamic Diameter Measurements. Part 1: Theory, *Aerosol Sci. Technol.* 38:1185–1205.

Dusek, U., Reischl, G. P., and Hitzenberger, R. (2006). CCN Activation of Pure and Coated Carbon Black Particles, *Environ. Sci. Technol.* 40, 1223–1230.

Flagan, R. C. (1999). On Differential Mobility Analyzer Resolution, *Aerosol Sci. Technol.* 30(6):556.

Fuller, K. A., Malm, W. C., and Kreidenweis, S. M. (1999). Effects of Mixing on Extinction by Carbonaceous Particles. *J. Geophys. Res.* 104, 15941–15954.

Fung, K. (1990). Particulate Carbon Speciation by MnO_2 Oxidation, *Aerosol Sci. Technol.* 12:122–127.

Gao, R. S., Schwarz, J. P., Kelly, K. K., Fahey, D. W., Watts, L. A., Thompson, T. L., Spackman, J. R., Slowik, J. G., Cross, E. S., Han, J.-H., Davidovits, P., Onasch, T. B., and Worsnop, D. R. (2007). A Novel Method for Estimating Light-Scattering Properties of Soot Aerosols Using a Modified Single-Particle Soot Photometer, *Aerosol Sci. Technol.* 41(2):125–135.

Gerber, H. E. (1982a). Absorption of Light by Atmospheric Aerosol Particles: Review of Instrumentation and Measurements. In *Light Absorption by Aerosol Particles*, ed. H. E. Gerber and E. E. Hindman, Technical Proceedings of the First International Workshop on Light Absorption by Aerosol Particles, Spectrum Press, Hampton, VA, pp. 21–43.

Gerber, H. E. (1982b). Optical Techniques for the Measurement of Light Absorption by Particulates, In *Particulate Carbon, Atmospheric Life Cycle*, ed. G. T. Wolff and R. Klimisch, Plenum Press, New York.

Gundel, L. A., Dod, R. L., Rosen, H., and Novakov, T. (1984). The Relationship Between Optical Attenuation and Black Carbon Concentration for Ambient and Source Particles, *Sci. Total Environ.* 36:197–202.

Hansen, A. D. A., Rosen, H., and Novakov, T. (1984). The Aethalometer—An Instrument for the Real-Time Measurement of Optical Absorption by Aerosol Particles, *Sci. Total. Environ.* 36:191–196.

Hansen, J., and Nazarenko, L. (2004). Soot Climate Forcing via Snow and Ice Albedos, *Proc. Natl. Acad. Sci.* 101(2):423–428.

Horvath, H. (1993). Atmospheric Light Absorption—A Review, *Atmos. Environ., Part A* 27:293–317.

Horvath, H., Catalan, L., and Trier, A. (1997). A Study of the Aerosol of Santiago de Chile III: Light Absorption Measurements, *Atmos. Environ.* 31:3737–3744.

Huntzicker, J. J., Jonson, R. L, Shaw, J. J., and Cary, R. A. (1982). Analysis of Organic and Elemental Carbon in Ambient Aerosols by a Thermal-Optical Method. In *Particulate Carbon: Atmospheric Life Cycle*, ed. Wolff, G. T., Klimisch, R. L., Plenum Press: New York, pp. 79–88.

IPCC (2001). "Third Assessment Report—Climate Change 2001," the third assessment report of the Intergovernmental Panel on Climate Change, IPCC/WMO/UNEP.

Jayne, J. T., Leard, D. C., Zhang, X., Davidovits, P., Smith, K. A., Kolb, C. E., and Worsnop, D. R. (2000). Development of an Aerosol Mass Spectrometer for Size and Composition Analysis of Submicron Particles, *Aerosol Sci. Technol.* 33:49–70.

Jimenez, J. L., Jayne, J. T., Shi, Q., Kolb, C. E., Worsnop, D. R., Yourshaw, I., Seinfeld, J. H., Flagan, R. C., Zhang, X., Smith, K. A., Morris, J., and Davidovits, P. (2003). Ambient Aerosol Sampling with an Aerosol Mass Spectrometer, *J. Geophys. Res.-Atmospheres*, 108(D7):8425.

Johnson, B. T. (2005). Large-Eddy Simulations of the Semidirect Aerosol Effect in Shallow Cumulus Regimes, *J. Geophys. Res.-Atmospheres.* 110(D14):14206.

Kleeman, M. J., Schauer, J. J., and Cass, G. R. (2000). Size and Composition Distribution of Fine Particulate Matter Emitted from Motor Vehicles, *Environ. Sci. Technol.* 34(7):1132–1142.

Moosmüller, H., Arnott, W. P., Rogers, C. F., Bowen, J. L., Gillies, J. A., Pierson, W. R., Collins, J. F., Durbin, T. D., and Norbeck, J. M. (2001). Time-Resolved Characterization of Diesel Particulate Emissions. 2. Instruments for Elemental and Organic Carbon Measurements, *Environ. Sci. Technol.* 35(10):1935–1942.

Moosmüller, H., Varma, R., and Arnott, W. P. (2005). Cavity Ring-Down and Cavity-Enhanced Detection Techniques for the Measurement of Aerosol Extinction, *Aerosol Sci. Technol.* 39:30–39.

Park, K., Cao, F., Kittelson, D. B., and McMurry, P. H. (2003). Relationship between Particle Mass and Mobility for Diesel Exhaust Particles, *Environ. Sci. Technol.* 37(3):577–583.

Penner, J. E., Zhang, S. Y., and Chuang, C. C. (2003). Soot and Smoke Aerosol May Not Warm Climate, *J. Geophys. Res.-Atmospheres* 108(D21):4657.

Petzold, A., Kramer, H., and Schonlinner, M. (2002). Continuous Measurement of Atmospheric Black Carbon Using a Multi-angle Absorption Photometer, *Environ. Sci. & Pollut. Res., Special Issue.* 4:78–72.

Petzold, A., and Schönlinner, M. (2004). Multi-Angle Absorption Photometer—A New Method for the Measurement of Aerosol Light Absorption and Atmospheric Black Carbon, *J. Aerosol Sci.* 35:421–441.

Petzold, A., Schloesser, H., Sheridan, P. J., Arnott, W. P., Ogren, J. A., and Virkkula, A. (2005). Evaluation of Multi-Angle Absorption Photometry for Measuring Aerosol Light Absorption, *Aerosol Sci. Technol.* 39:40–51.

Reid, J. S., Hobbs, P. V., Liousse, C., Martins, J. V., Weiss, R. E., and Eck, T. F. (1998). Comparisons of Techniques for Measuring Shortwave Absorption and Black Carbon Content of Aerosols from Biomass Burning in Brazil, *J. Geophys. Res.—Atmospheres.* 103(D24):32031–32040.

Rosencwaig, A. (1980). *Photoacoustics and Photoacoustic Spectroscopy*. Wiley, New York.

Saathoff, H., Möhler, O., Schurath, U., Kamm, S., Dippel, B., and Mihelcic, D. (2003a). The AIDA Soot Aerosol Characterisation Campaign 1999, *J. Aerosol Sci.* 34: 1277–1296.

Saathoff, H., Naumann, K.-H., Schnaiter, M., Schöck, W., Möhler, O., Schurath, U., Weingartner, E., Gysel, M., and Baltensperger, U. (2003b). Coating of Soot and $(NH_4)_2SO_4$ Particles by Ozonolysis Products of α-Pinene, *J. Aerosol Sci.* 34:1297–1321.

Schmid, H., Laskus, L., Abraham, J. H., Baltensperger, U., Lavanchy, V., Bizjak, M., Burba, P., Cachier, H., Crow, D., Chow, J., Gnauk, T., Even, A., ten Brink, H. M., Giesen, K.-P., Hitzenberger, R., Hueglin, C., Maenhaut, W., Pio, C., Carvalho, A., Putaud, J.-P., Toom-Sauntry, D., and Puxbaum, H. (2001). Results of the "Carbon Conference" International Aerosol Round Robin Test Stage I, *Atmos. Environ.* 35:2111–2121.

Schnaiter, M., Horvath, H., Möhler, O., Naumann, K.-H., Saathoff, H., and Schöck, O. W. (2003). UV-VIS-NIR Spectral Optical Properties of Soot and Soot-Containing Aerosols, *J. Aerosol Sci.* 34:1421–1444.

Schwarz, J. P., Gao, R. S., Fahey, D. W., Thomson, D. S., Watts, L. A., Wilson, J. C., Reeves, J. M., Baumgardner, D. G., Kok, G. L., Chung, S., Schulz, M., Hendricks, J., Lauer, A., Kärcher, B., Slowik, J. G., Rosenlof, K. H., Thompson, T. L., Langford, A. O., Lowenstein, M., and Aikin, K. C. (2006). Single-Particle Measurements of Midlatitude Black Carbon and Light-Scattering Aerosols from the Boundary Layer to the Lower Stratosphere. *J. Geophys. Res.* 111:D16207. doi:10.1029/2006JD007076.

Sharma, S., Brook, J. R., Cachier, H., Chow, J., Gaudenzi, A., and Lu, G. (2002). Light Absorption and Thermal Measurements of Black Carbon in Different Regions of Canada, *J. Geophys. Res.—Atmospheres.* 107(D24):4771.

Sheridan, P. J., Arnott, W. P., Ogren, J. A., Andrews, E., Atkinson, D. B., Covert, D. S., Moosmüller, H., Petzold, A., Schmid, B., Strawa, A. W., Varma, R., and Virkkula, A. (2005). The Reno Aerosol Optics Study: An Evaluation of Aerosol Absorption Measurement Methods, *Aerosol Sci. Technol.* 39:1–16.

Slowik, J. G., Stainken, K., Davidovits, P., Williams, L. R., Jayne, J. T., Kolb, C. E., Worsnop, D. R., Rudich, Y., DeCarlo, P., and Jimenez, J. L. (2004). Particle Morphology and Density Characterization by Combined Mobility and Aerodynamic Diameter Measurements. Part 2: Application to Combustion Generated Soot Particles as a Function of Fuel Equivalence Ratio, *Aerosol Sci. Technol.* 38:1206–1222.

Slowik, J. G., Han, J.-H., Kolucki, J., Davidovits, P., Williams, L. R., Onasch, T. B., Jayne, J. T., Kolb, C. E., and Worsnop, D. R. (2007). Effect of Organic Species Condensation on Soot Particle Morphology. *Aerosol Sci. Technol.*, submitted.

Smith, J. D., and Atkinson, D. B. (2001). A Portable Pulsed Cavity Ring-Down Transmissometer for Measurement of the Optical Extinction of the Atmospheric Aerosol, *Analyst.* 126(8):1216–1220.

Stephens, M., Turner, N., and Sandberg, J. (2003). Particle Identification by Laser-Induced Incandescence in a Solid-State Laser Cavity, *Applied Optics* 42(19):3726–3736.

Turpin, B. J., Cary, R. A., and Huntzicker, J. J. (1990). An In Situ, Time-Resolved Analyzer for Aerosol Organic and Elemental Carbon, *Aerosol Sci. Technol.* 12:161–171.

VDI 2465 Part 1 (1996). Measurement of Soot (Immission) Chemical Analysis of Elemental Carbon by Extraction and Thermal Desorption of Organic Carbon. VDI/DIN-Handbuch Reinhaltung der Luft 4.

Viidanoja, J., Kerminen, V.-M., and Hillamo, R. (2002). Measuring the Size Distribution of Atmospheric Organic and Black Carbon Using Impactor Sampling Coupled with Thermal Carbon Analysis: Method Development and Uncertainties, *Aerosol Sci. Technol.* 36:607–616.

Virkkula, A., Ahlquist, N. C., Covert, D. S., Arnott, W. P., Sheridan, P. J., Quinn, P. K., and Coffman, D. J. (2005). Modification, Calibration, and a Field Test of an Instrument for Measuring Light Absorption by Particles, *Aerosol Sci. Technol.* 39:68–83.

APPENDIX A

To understand the difference in the absorption measurements provided by the MAAP and PAS for uncoated soot and GC spheres, two factors must be considered: (1) The optical absorption of the BC/GC material depends inversely on wavelength; and (2) For particles of a given material with a diameter on the order of the wavelength of light, the absorption depends on the relative magnitudes of the diameter and wavelength. Here we consider the effect of these factors on the MAAP and PAS measurements of absorption via their effect on the mass-specific absorption coefficient, σ_{abs}.

The simplest case to consider is that of the fractal soot particles. In the soot aggregates, each spherule absorbs light individually. Because these spherules (diameter = 30–40 nm) are small relative to the wavelength of light used by the MAAP and PAS (670 nm and 870 nm, respectively), σ_{abs} is independent of particle size. For these particles, only the first factor given above (i.e., inverse wavelength dependence) must be considered to compare the MAAP and PAS measurements.

We now consider the absorption of the GC spheres at a single arbitrary wavelength on the order of the wavelengths used by the MAAP and PAS. Because these the diameter of these particles (165 to 460 nm) is on the order of the wavelengths used by the measuring instruments, only the particle skin participates in light absorption. Within this layer, σ_{abs} is unchanged from the small particle case discussed in the previous paragraph. However, because the amount of potentially absorbing but optically inaccessible material increases with particle diameter, the

measured σ_{abs} decreases approximately as d^{-1} (see for example Bond and Bergstrom 2006; Fuller et al. 1999; Horvath 1993). A crucial difference between the MAAP and the PAS measurement of the GC spheres is that because the skin depth increases with wavelength, the d^{-1} dependence of σ_{abs} is less pronounced for the PAS (measuring at wavelength = 870 nm) than for the MAAP (wavelength = 670 nm).

To fully compare the MAAP and PAS absorption measurements for the GC spheres and uncoated soot, the inverse wavelength and inverse diameter dependences (factors 1 and 2 above) must be treated simultaneously. In Figure A1, we show σ_{abs} as a function of particle diameter for as measured by the MAAP and PAS instruments. To parallel the treatment of the measurements of these instruments in the body of the paper, the MAAP measurement has been converted to 870 nm assuming inverse wavelength dependence. However, in light of the discussion in the previous paragraph, we must stress the important distinction between directly measuring σ_{abs} at 870 nm (PAS) and converting a measurement at 670 nm to 870 nm (MAAP).

Figure A1 is constructed from the calculations of Fuller et al. (1999) as follows. Fuller et al. present calculations of σ_{abs} for diesel soot (refractive index $= 2.00 + 1.00i$) at 550 nm. We convert their measurements to 670 nm (MAAP) and 870 nm (PAS) in three steps. (1) We assume inverse wavelength dependence for the absorbing material (factor 1 above). (2) We account for the effect of particle size on σ_{abs} (factor 2 above) by assuming that σ_{abs} is a function of the ratio of diameter to wavelength. That is, σ_{abs} (d = 200 nm, λ = 200) = σ_{abs} (d = 400 nm, $\lambda = 400$). (3) We convert the MAAP measurement of σ_{abs} from λ = 670 nm to λ = 870 nm The observed experimental results for GC spheres are in accord with the response shown in Figure A1. Specifically, with the MAAP absorption measurement for fractal soot a factor of 1.2 higher than the PAS measurement, σ_{abs} in the range of the GC sphere diameter is shown to be in the range 0.9-1.0 for the MAAP relative to the PAS. The peak in σ_{abs} evident for both the MAAP and PAS was not discussed above and is due to dipolar resonance modes in the spherical particles (Fuller et al. 1999).

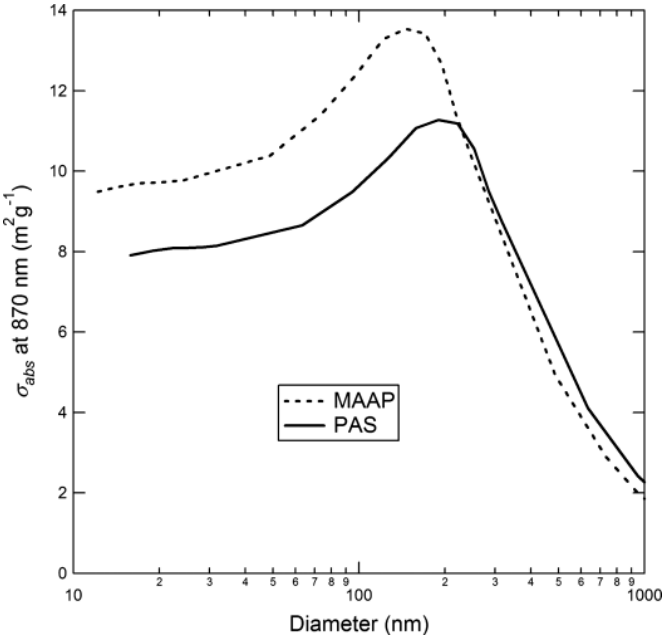

FIG. A1. Model mass-specific absorption coefficient (σ_{abs}) at 870 nm measured by the MAAP and PAS as a function of particle diameter. See text for a discussion of the assumptions and methods used to generate this figure.